

Analysis of Multiresolution Data Fusion Techniques

Duane B. Carter

Thesis submitted to the Faculty of the
Virginia Polytechnic Institute and State University
in partial fulfillment of the requirements for the degree of

Master of Science in Geography

Dr. James B. Campbell, Chair
Dr. John Randolph
Dr. Randolph H. Wynne

March 23, 1998
Blacksburg, Virginia

Analysis of Multiresolution Data Fusion Techniques

Duane B. Carter

(ABSTRACT)

In recent years, as the availability of remote sensing imagery of varying resolution has increased, merging images of differing spatial resolution has become a significant operation in the field of digital remote sensing. This practice, known as data fusion, is designed to enhance the spatial resolution of multispectral images by merging a relatively coarse-resolution image with a higher resolution panchromatic image of the same geographic area. This study examines properties of fused images and their ability to preserve the spectral integrity of the original image. It analyzes five current data fusion techniques as applied to three complex scenes to assess their performance. The five data fusion models used include one spatial domain model (High-Pass Filter), two algebraic models (Multiplicative and Brovey Transform), and two spectral domain models (Principal Components Transform and Intensity-Hue-Saturation). SPOT data were chosen for both the panchromatic and multispectral data sets. These data sets were chosen for the high spatial resolution of the panchromatic (10 meters) data, the relatively high spectral resolution of the multispectral data, and the low spatial resolution ratio of two to one (2:1). After the application of the data fusion techniques, each merged image was analyzed statistically, graphically, and for increased photointerpretive potential as compared with the original multispectral images. While all of the data fusion models distorted the original multispectral imagery to an extent, both the Intensity-Hue-Saturation Model and the High-Pass Filter model maintained the original qualities of the multispectral imagery at the highest level. The High-Pass Filter model, designed to highlight the high frequency spatial information, provided the most noticeable increase in spatial resolution.

Acknowledgments

“A man’s life is merely a collection of events, building one upon the other. When all the events are tallied; the triumphs; the failures; the mistakes, their sum makes up the man.”

Neal Cassady

I would like to thank my committee members Jim Campbell for providing me with insight and foresight both in the development of this thesis and in general; Randy Wynne for the excitement and enthusiasm he has brought to me toward the field of remote sensing; and, John Randolph for giving me the ability to see humor in all aspects of life in academia. I would also like to give a special thanks to my fellow graduate students and the staff of the Geography Department, Richard Easterbrook, Bob Heselton, Mannin Dodd, John Boyer, Chris Ratigan, Jane Price and Vanessa Scott for their support and guidance for the past two years. Yet, this thesis is but one mere triumph in this individual’s life and would be incomplete without giving respect to my mother, LaVonna B. John, who has stood by me through the failures and mistakes as well as the triumphs.

Table of Contents

Abstract	ii
Acknowledgments	iii
List of Figures	v
List of Tables	vii
Chapter One: Introduction	1
Spatial and Spectral resolution	1
The Factor of Scale	2
Advantages of Data Fusion	2
Applications	3
Data Characteristics	5
Test Area's	6
Research Goals	7
Chapter Two: Data Fusion Models	8
Rectification and Registration	8
High-Pass Filter Model	9
Multiplicative Model	10
Brovey Transform	10
Principal Components Transformation	10
Intensity-Hue-Saturation	12
Chapter Three: Methods of Evaluation	15
Methods of Evaluation	15
Chapter Four: Results and Analysis	18
Discussion	
Chapter Five: Conclusion	38
Appendix A: F Test Results	42
Appendix B: Photointerpretive Evaluation	45
Appendix C: Results of Photointerpretive Evaluation	46
Appendix D: Results of ANOVA: two way without replication	49
Bibliography	51
Vita	52

List of Figures

Figure Number	Description	Page
Figure 1:	SPOT XS image of the Blacksburg, Virginia area.	6
Figure 2:	SPOT PN image of the Blacksburg, Virginia area.	6
Figure 3:	SPOT XS image of the Laguna Beach, California area.	6
Figure 4:	SPOT PN image of the Laguna Beach, California area.	6
Figure 5:	SPOT XS image of the Seattle, Washington area.	6
Figure 6:	SPOT PN image of the Seattle, Washington area.	6
Figure 7:	Relationship between Spot Panchromatic Pixel and Spot Multispectral pixel.	9
Figure 8:	Schematic diagram of the HPF Model.	9
Figure 9:	Schematic diagram of the PCT Model.	11
Figure 10:	Schematic diagram of the IHS Model.	12
Figure 11:	HPF model for Blacksburg, Virginia area.	18
Figure 12:	MLT model for Blacksburg, Virginia area.	18
Figure 13:	BT model for Blacksburg, Virginia area.	18
Figure 14:	PCT model for Blacksburg, Virginia area.	18
Figure 15:	IHS model for Blacksburg, Virginia area.	18
Figure 16:	HPF model for Laguna Beach, California area.	18
Figure 17:	MLT model for Laguna Beach, California area.	18
Figure 18:	BT model for Laguna Beach, California area.	18
Figure 19:	PCT model for Laguna Beach, California area.	18
Figure 20:	IHS model for Laguna Beach, California area.	18
Figure 21:	HPF model for Seattle, Washington area.	18
Figure 22:	MLT model for Seattle, Washington area.	18
Figure 23:	BT model for Seattle, Washington area.	18
Figure 24:	PCT model for Seattle, Washington area.	18
Figure 25:	IHS model for Seattle, Washington area.	18
Figure 26:	Blacksburg mean brightness values for original XS image and the five data fusion models..	20
Figure 27:	Laguna Beach mean brightness values for original XS image and the five data fusion models.	20
Figure 28:	Seattle mean brightness values for original XS image and the five data fusion models.	20
Figure 29:	Feature space plots of band 2 versus band 3 of the Blacksburg data fusion models as compared with the original data.	32

Figure 30:	Feature space plots of band 2 versus band 3 of the Laguna Beach data fusion models as compared with the original data.	32
Figure 31:	Feature space plots of band 2 versus band 3 of the Seattle data fusion models as compared with the original data.	32
Figure 32:	Urban Spectral Plot for Blacksburg data fusion models.	33
Figure 33:	Agricultural Spectral Plot for Blacksburg data fusion models.	33
Figure 34:	Deciduous forest Spectral Plot for Blacksburg data fusion models.	33
Figure 35:	Urban Spectral Plot for Laguna Beach data fusion models.	34
Figure 36:	Agricultural Spectral Plot for Laguna Beach data fusion models.	34
Figure 37:	Water Spectral Plot for Laguna Beach data fusion models.	34
Figure 38:	Urban Spectral Plot for Seattle data fusion models.	35
Figure 39:	Water Spectral Plot for Seattle data fusion models.	35
Figure 40:	Coniferous Spectral Plot for Seattle data fusion models.	35
Figure 41:	Data Fusion Flow Chart	39

List of Tables

Table Number	Description	Page
Table 1:	Applications of Data Fusion and requirements that must be met for a data fusion model to be practical.	4
Table 2:	Informational content of the Blacksburg, Laguna Beach, and Seattle data sets.	7
Table 3:	Correlation between Panchromatic data, Intensity channel, Principal Component 1, XS 1, and XS 2 for the Laguna Beach Scene.	12
Table 4:	Means and Standard Deviations for the three scene's multispectral data and the resultant data fusion models.	19
Table 5:	Variance/covariance matrix for the Blacksburg data fusion models.	21
Table 6:	Correlation matrix for the Blacksburg data fusion models.	22
Table 7:	Variance/covariance matrix for the Laguna Beach data fusion models.	23
Table 8:	Correlation matrix for the Laguna Beach data fusion models.	24
Table 9:	Variance/covariance matrix for the Seattle data fusion models.	25
Table 10:	Correlation matrix for the Seattle data fusion models.	26
Table 11:	Spectral Root Mean Square Errors for the Blacksburg data fusion models.	27
Table 12:	Spectral Root Mean Square Errors for the Laguna Beach data fusion models.	28
Table 13:	Spectral Root Mean Square Errors for the Seattle data fusion models.	29
Table 14:	Summary of Statistical Results by model as compared with each scene's original XS image.	31
Table 15:	Per scene, per model, and average overall responses for the photointerpretive survey.	37
Table 16:	Hierarchy of Data Fusion Models by Discipline.	40

CHAPTER ONE

INTRODUCTION

Multiresolution data fusion, also known as data merging or pan sharpening, has become an important aspect of digital remote sensing over the past two decades. Enhancing multispectral data sets with the higher spatial resolution of panchromatic images, radar imagery, and digitized aerial photographs can increase photointerpretive potential as well as improve analytical capabilities. Because the main intent of data fusion has been to enhance the spatial resolution of a multispectral image, preservation of spectral integrity has often been neglected. This study examines some of the more widely used data fusion models by assessing their ability to preserve spectral integrity.

Spatial and Spectral Resolution

Spatial resolution is the clarity of high frequency information of an image and is interdependent with scale. Spatial resolution is often expressed as the width of the instantaneous field of view (IFOV), or one side of a pixel (picture element). The IFOV is the ground area sensed by a sensor at an instant in time (Lillesand and Kiefer, 1994). The finer or smaller the IFOV, the higher the spatial resolution. Each digital image is formed as an array of pixels, where each pixel contains specific information about a scene. Although, it is possible to resample (i.e., aggregate or subdivide pixels) an image so that the pixel size becomes smaller than the original's spatial dimensions, its informational content retains the original data's spatial resolution (Campbell, 1996).

Spectral resolution is defined as the width within the electromagnetic spectrum that can be detected by a band of a sensor. The narrower the spectral bandwidth, the higher the spectral resolution. Usually, finer spectral resolution requires a larger IFOV (coarser spatial resolution), in order to maintain a sufficient level of energy reaching the sensor's detector. All other factors held constant, a larger IFOV results in a longer measurement time over a given ground resolution cell and a higher signal-to-noise ratio (SNR), that is a signal that is much greater than the background electronic noise associated with any given system (Lillesand and Kiefer, 1994).

Thus, imaging systems are designed to balance two competing constraints--spatial resolution and signal-to-noise ratio (SNR). Multispectral and hyperspectral systems have reduced bandwidths which require a coarser IFOV in order to collect enough photons to maintain an acceptable SNR. Panchromatic sensors usually have broader spectral bandwidths, which allows for finer spatial resolution by increasing the SNR over a broad spectral band (Schowengerdt, 1997). Thus, to increase either spectral or spatial resolution one of the two must be sacrificed. Data fusion is an image processing technique that might allow analysts to circumvent this trade off and permit preservation of fine resolution and spectral integrity.

The Factor of Scale

The factors of scale and spatial resolution are intimately related, in that scale of an image map is limited by the clarity or spatial resolution of the image. Selecting an appropriate scale for scientific investigations is an important step in deciding what spatial resolution is necessary (Woodcock and Strahler, 1987). Current sensors have a wide distribution of spatial resolutions, which vary over many orders of magnitude--from the IRS-1C's (Indian Remote Sensing-1C) 5-meter resolution to the AVHRR's (Advanced Very High Resolution Radiometer) 1.1- and 4-km resolution, not to mention the future generation of 1-meter and sub-meter high resolution satellites scheduled for launch (Atkinson and Curran, 1997). So, before deciding which data fusion technique to use, as will be discussed later, it is essential that analysts understand which level of detail is appropriate for a given analysis.

The appropriate scale varies with the type of environment being analyzed, the information desired, and the level of detail necessary. Analytical and interpretive techniques used to extract information from the data sets must also be considered. Because of the limiting factor of spatial resolution available from space-borne sensors, analysts are limited in their choices. Strahler et al. (1986), describe two resolution models that can be effective in determining which resolution and thus which scale is appropriate. The H- and L- resolution models are essentially based on whether the elements being remotely sensed are larger or smaller than the resolution cells respectively. The use of H- and L- as opposed to high and low is to separate the absolute measurement of spatial resolution verse the relative size of elements as compared to the spatial resolution of a sensor. If an analyst needs a regional overview, a L-resolution image would be allowable. If an analyst needs detailed linear features and point features a H-resolution model would be necessary. Thus, the major factors that should be considered when choosing an appropriate scale, and hence a data fusion technique, are the information desired from the imagery, the analytical and interpretive methods used to extract the information, and the spatial resolution of the scene itself (Woodcock and Strahler, 1987).

Advantages of Data Fusion

Data fusion provides several advantages: preservation of computer storage space; enhancement of aesthetic and cosmetic qualities; improvement of spatial resolution; and, analytical improvements. Each reason for data fusion relies on the following premise--for a data fusion model to be effective, the merged images should retain the high spatial resolution information from the panchromatic data set while maintaining the basic spectral record of the original multispectral data (Carper et al, 1990).

Computer storage is becoming less of a constraint in gathering and analyzing digital data than in previous years, but still remains a major obstacle. In 1977, Colvocoresses proposed a combination of high spatial resolution spectral bands and lower resolution bands to reduce storage demands without sacrificing informational content of the imagery for the Landsat mission. Similarly, Schowengerdt (1980) proposed a combination of low spatial resolution spectral channels and one

higher spatial resolution channel to carry high frequency spatial information common to all channels. These data sets could later be merged for analysis. With the advent of the new generation of high resolution commercial satellites, combinations of panchromatic data and multispectral data will significantly enhance the clarity of the imagery while decreasing storage space required on the satellite system, the ground stations, and office equipment (Wynne and Carter, 1997).

Gehring and Perry (1979) combined data for aesthetic enhancement when they created color composites of RBV (Return Beam Vidicon) and MSS (Multispectral Scanner) data. By adding the aspect of color to a fine resolution image the photointerpretive potential is increased (Robinson et al, 1995). When data sets are combined, even if spectral qualities are not completely preserved, the added color aids photointerpretive potential more than a simple gray-scale panchromatic scene.

Yet, data fusion has also increased the scientific uses of data. The major scientific contribution of data fusion by far has been the increased cartographic potential of the merged data sets. In 1978, Daily et al merged SIR-A (Shuttle Imaging Radar-A) data with MSS data for geologic mapping of Death Valley in California. Data fusion has since been used for a variety of mapping application such as by Chavez (1986) for 1:24,000 scale mapping, by Ford and Mckeown (1992) for cartographic feature extraction, by Grasso (1993) for 1:24,000 geologic mapping, by Pohl and van Genderen (1995) to update topographic maps in the tropics, and by Munechika et al (1993) to improve classification accuracy. The analytical and photointerpretive capabilities provided by merging two complimentary data sets are quite evident in the preceding studies.

Applications

Data fusion can be used to enhance data for use in a variety of environmental, planning, and resource related studies. For environmental disciplines, it can increase the effectiveness of environmental impact assessments that require remotely sensed imagery, such as coastal zone monitoring, fluvial geomorphology, and flood plain mapping. Planning disciplines often make use of remotely sensed imagery and with increased resolution and spectral enhancements practices such as producing land use/land cover maps can be augmented. Resource related disciplines deal with both renewable and non-renewable resources. Renewable resources, including agriculture and forestry, already use aerial photography intensively and can benefit from the higher spatial resolution when spectral integrity is maintained. Data fusion is also readily applicable to non-renewable resources such as geology, soils, and archaeology where synoptic overviews and spectral differentiation are necessary. This study will analyze data fusion techniques as applicable to environmental, planning, agriculture, forestry, geology, and cartography (Table 1).

Environmental Monitoring

Effective analysis of environmental issues consistently requires use of remotely sensed imagery. Issues such as wetlands and habitat delineation, coastal zone monitoring, flood plain mapping, and resource assessment are of concern for maintaining environmental health and hazards management. For remotely sensed imagery, and thus, data fusion models, to be effective for

Table 1: Applications of Data Fusion and requirements that must be met for a data fusion model to be practical.

APPLICATIONS	REQUIREMENTS
Environmental Monitoring	High Spatial Resolution, Spectral Integrity, Co-temporal imagery, and Repeat Coverage
Planning	High Spatial Resolution and Broad Areal Coverage
Agriculture	High Spatial Resolution, Spectral Integrity, Co-temporal imagery, and Repeat Coverage
Forestry	High Spatial Resolution, Spectral Integrity, Co-temporal imagery, and Repeat Coverage
Geology	High Spatial Resolution, Spectral Differentiation, with spectral bands within the 1.6 μ m and 2.2 μ m wavelengths
Cartography	High Spatial Resolution and Spectral Differentiation

environmental management they must provide synoptic overviews of areas of interest, high spatial resolution, good spectral resolution and integrity, and the ability to have repeat coverage and co-temporal data sets.

Planning

Planning encompasses both urban planning and rural/regional planning. Land use/land cover maps have often been the main use of remote sensing for planning. Other uses have included siting studies and cultural/demographic change detection. The requirements for data fusion models to be applicable to planning are high spatial resolution and broad areal coverage. For planning, and urban planning especially, the spectral requirements are not as dominant as for other disciplines. What this means, is that a spectrally enhanced high spatial resolution image will increase the planner's ability to perform the tasks listed above without major concerns for spectral integrity.

Agriculture

Satellite and aerial photography have been valuable resources to large scale agriculture. Crop forecasting, crop inventory, production monitoring, soil moisture assessments/irrigation requirements, and crop damage assessments from episodal events are greatly enhanced with the synoptic overviews provided by remotely sensed imagery. For a data fusion technique to be viable for agriculture, the increased spatial resolution must also be complimented by high spectral integrity, specifically within the red and near infrared wavelengths, and there must be frequent repeat coverage with co-temporal data.

Forestry

As with agriculture, foresters have also benefitted from the use of remotely sensed imagery. Foresters use imagery to conduct forest inventories, plan harvest logistics, prepare stand density calculations, make disease and fire damage assessments, and use as a tool for preventive and predictive fire management. Similar to above, the increased spatial resolution provided by a data fusion technique must also maintain spectral integrity to a high degree to be of use for forestry.

Geology

The broad overview provided by aerial imagery has provided geologists with tools that have enhanced structural mapping, tectonic studies, lithological studies, and along with environmental disciplines an increased ability to understand geologic hazards and to conduct hazard analysis. The higher spatial resolution and spectral differentiation provided by data fusion techniques increase the interpretability of imagery for geology. Satellite data also provides an increased spectral range, by sensing within the $1.6\mu\text{m}$ and $2.2\mu\text{m}$ wavelengths which are valuable for geologic studies. Although this paper does not study the spectral channels useful to geologists provided by the Thematic Mapper (TM), the techniques examined here are still applicable for data fusion of higher resolution imagery and TM data as shown by Chavez (1986).

Cartography

Cartographic applications of data fusion have formed the dominant use of data fusion techniques. Topographic mapping, terrain modeling, and map updating benefit from the increased spatial resolution and spectral enhancements provided by merging two complimentary data sets. Requirements for spectral integrity for cartographic applications vary with the type of mapping, but spectrally enhanced fine resolution products increase cartographic potential.

Data Characteristics

All data sets used for this study were collected by SPOT satellites using HRV (high resolution visible) sensors in both the panchromatic (PN) mode and the multispectral (XS) mode. The spatial resolution of the sensor varies with which mode the data was acquired in. In the PN mode the spatial resolution is 10-meters within the spectral range of $0.51\mu\text{m}$ to $0.73\mu\text{m}$. In the XS configuration the spatial resolution is 20-meters and senses three spectral regions:

- Band 1: 0.50 to $0.59\mu\text{m}$ (green)
- Band 2: 0.61 to $0.68\mu\text{m}$ (red)
- Band 3: 0.79 to $0.89\mu\text{m}$ (near infrared)

(Campbell, 1996).

SPOT data were chosen for three reasons, the high spatial resolution of the panchromatic

images, the relatively high spectral resolution of the multispectral images, and the relatively low spatial resolution ratio of two to one (2:1). Also, of note is the ability of the SPOT sensors to gather co-temporal images. Co-temporal scenes, scenes acquired on the same day and time, reduce the need for radiometric normalization between scenes and also eliminates cultural and natural differences between scenes, e.g., construction or differences in vegetation cycles. The spatial resolution ratio is the ratio of the spatial resolution of two sets of imagery. The low resolution ratio of SPOT PN and XS data allows the analyst to use a nearest-neighbor resampling technique which reduces the change in brightness values (BV) within the XS image. Concerns of this nature, discussed in chapter two, are increased when data of differing dates and larger spatial resolution ratios are used for data fusion.

Test Areas

Three test areas and six data sets were chosen for this study. The area covered by the first two data sets is of the Blacksburg, Virginia area; the Virginia Tech campus is at the upper right of this scene with Price's Mountain toward the center left and Brush Mountain at the top left of the scene (Figure 1 and 2). Acquisition dates for the Blacksburg scenes are March 19, 1995 for the panchromatic scene and April 9, 1995 for the multispectral scene. Both images were processed to Level 1B by the SPOT processing system. The XS and PN images were subset to correspond to the Blacksburg 7.5 minute USGS quadrangle. The resultant image sizes were 576 columns by 726 rows for the XS and 1152 columns by 1452 rows for the PN.

The second two data sets are of the Laguna Beach, California area, both acquired on April 4, 1993, and have noticeable fire scars from the Laguna Beach fires of 1993 (Figure 3 and 4). The third data sets are of the Seattle, Washington metropolitan area (Figure 5 and 6). The panchromatic data set was acquired May 16 and the multispectral data set was acquired April 14, 1993. All four of the data sets were processed to Level 3A of the SPOT processing system. The XS images were subset to 1024 columns by 1024 rows and the PN images were subset to 2048 columns by 2048 rows.

Figure 1: SPOT XS image of the Blacksburg, Virginia area.

Figure 2: SPOT PN image of the Blacksburg, Virginia area.

Figure 3: SPOT XS image of the Laguna Beach, California area.

Figure 4: SPOT PN image of the Laguna Beach, California area.

Figure 5: SPOT XS image of the Seattle, Washington area.

Figure 6: SPOT PN image of the Seattle, Washington area.

Table 2: Informational content of the Blacksburg, Laguna Beach, and Seattle data sets.

Scene	Informational Content
Blacksburg, VA	Urban, Agricultural, and Mixed Deciduous Forest
Laguna Beach, CA	Urban, Agricultural, Water, and Fire Scars
Seattle, WA	Urban, Water, and Coniferous Urban Green space

Each area comprises a complex scene with a variety of elements. The Blacksburg scene contains urban, agricultural (cropland and pasture), and mixed deciduous forest elements. The Laguna Beach scene is composed of agricultural (cropland), urban, coastal areas, and fire scarred mountains. The Seattle scene is mainly urban, with a mixture of urban green space and coniferous trees, and the Puget Sound. These areas were chosen for their diversity of cultural and natural elements for the purpose of studying spectral responses over a variety of landscapes (Table 2).

Research Goals

This study will analyze five data fusion techniques, to be described in chapter two, based on their performance with respect to preservation of spectral integrity. The five techniques implemented in this study act upon the data sets within the spatial, algebraic, and spectral domains. Each data fusion model will then be analyzed using statistical, graphical, and photointerpretive tests, as explained in chapter three and presented in chapter four. These results will then be compiled and analyzed to provide potential users of data fusion techniques a look-up table listing of discipline related applications.

CHAPTER TWO

DATA FUSION MODELS

Five data fusion techniques were used for this analysis: one spatial domain model, two algebraic models, and two spectral domain models. *Spatial domain* models isolate the high frequency spatial information of the higher spatial resolution image, then combine that information with the multispectral data (Schowengerdt, 1997). The spatial domain model used here is the High-Pass Filter (HPF) Model and is similar to the one implemented by Chavez et al.(1991). *Algebraic models* operate on data sets using pixel by pixel arithmetic functions, such as addition, subtraction, multiplication and division. The two algebraic models used for this study are the Multiplicative Model (MLT) and the Brovey Transform (BT). *Spectral domain* models transform the multispectral (XS) imagery from spectral space into feature space, where one of the new images created by the transformation, defined below, is correlated with the Panchromatic (PN) data set. The two spectral domain models are the Principal Components Transformation (PCT) and the Intensity-Hue-Saturation (IHS) Model. These five models are among the most often used for data fusion. The test data sets were each subjected to each of the five data fusion techniques; the results were analyzed to evaluate their spectral integrity and photointerpretive potential.

Rectification and Registration

Before data fusion techniques can be applied to multispatial data, two important steps must occur: image rectification and image-to-image registration. First, one image must be rectified, then used as the master for registration of the other image. It is important to note that, although data sets should share a common planimetric format in order for data fusion to occur, the minimum requirement simply is that they are registered to each other to assure that the images are aligned.

Second, depending on the resolution-ratio, XS data must be digitally expanded so that the resultant pixel size is the same as the pixel size of the PN data. Expansion is typically accomplished by pixel duplication of the XS image. The SPOT data sets used for this study have a low resolution-ratio (Figure 7), an expansion factor of 2 yields the 10-meter pixel size desired. Since expansion of digital imagery yields coarser image detail, a low-pass filter can be implemented to smooth the resultant "blockiness" of the XS image. These data can then be registered to the PN data using a nearest neighbor resampling technique. A rule of thumb for choosing a resampling technique, is that the expanded number of pixels operated on during the resampling technique should match the resolution-ratio squared. For example, the SPOT XS registration to SPOT PN data, as used here, the ratio is 2:1, 2^2 is equal to 4, so a nearest neighbor technique was implemented; for Thematic Mapper (TM) registration to SPOT PN data the ratio is 3:1, 3^2 is equal to 9, so a bilinear interpolation technique would be used; accordingly, higher ratios--e.g., when merging TM images with digitized aerial photographs-- necessitate higher level resampling techniques and will result in increased generalization.

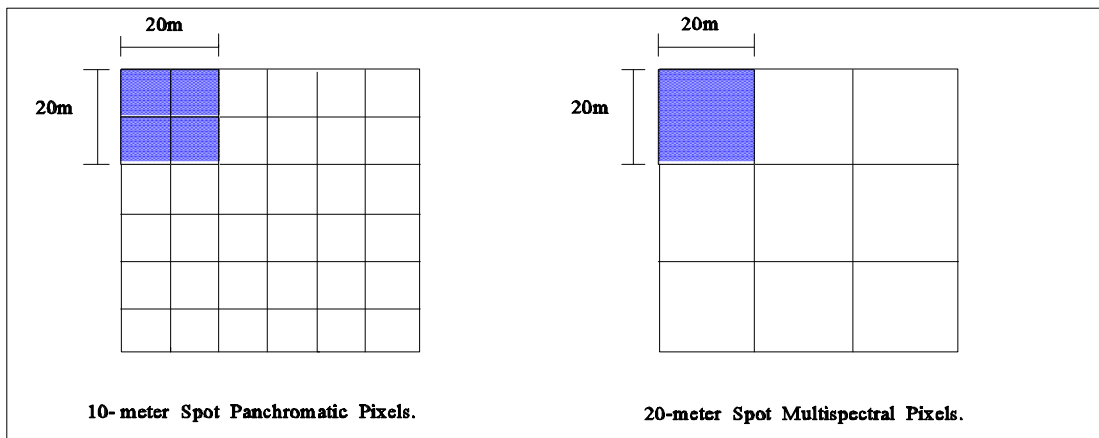


Figure 7: Relationship between SPOT Panchromatic Pixel and SPOT Multispectral pixel.

High-Pass Filter Model (HPF)

The High-Pass Filter model (figure 8) was first introduced by Schowengerdt (1980) as a method to reduce data quantity and increase spatial resolution potential for Landsat MSS data. Chavez et al. (1991) extended this idea to more diverse multispatial data sets when they merged Thematic Mapper (TM) data with a digitized National High Altitude Program (NHAP) aerial photograph. The HPF method submits the high spatial resolution imagery to a small convolution mask (3 x 3) which acts upon the high-frequency spatial information, effectively reducing the lower frequency spectral information of the high spatial resolution image. The filtered results (FP) are then

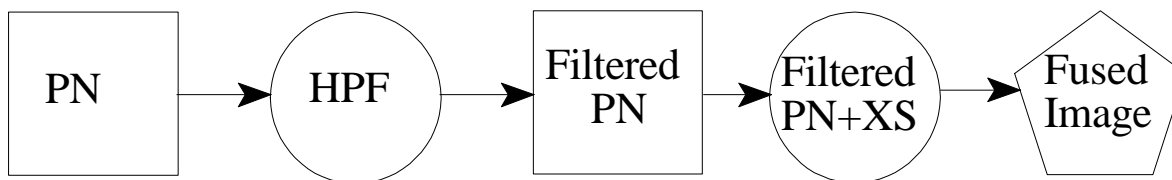


Figure 8: Schematic diagram of the HPF Model.

added to the XS data and the result divided by two to offset the increase in brightness values (eq. 2-1):

$$HPF_{i,j,k} = (XS_{i,j,k} + FP_{i,j})/2 \quad (2-1)$$

where HPF is the output image and i and j are pixels of band k. This technique preserves the XS data while incorporating the spatial resolution of the PN data.

Multiplicative Model (MLT)

The Multiplicative model combines two data sets by multiplying each pixel in each band of the XS data by the corresponding pixel of the PN data. To compensate for the increased BV's the square root of the mixed data set is taken. The square root of the multiplicative data set, reduces the data to a combination reflecting the mixed spectral properties of both data sets (eq. 2-2):

$$MLT_{i,j,k} = (XS_{i,j,k} \times PN_{i,j})^{1/2} \quad (2-2)$$

where MLT is the output image and i and j are pixels of band k. To compensate for this effect, weighting coefficients can be used. As Cliche and Bonn (1985, p. 316) noted, “however arbitrary, the weights used for the panchromatic and infrared channels increase the spatial resolution from 20 to 10 m and preserve much of the infrared information.”

Brovoy Transform (BT)

The Brovey Transform is a ratio method where the data values of each band of the XS data set are divided by the sum of the XS data set and then multiplied by the PN data set. The Brovey Transform attempts to maintain the spectral integrity of each band by incorporating the proportionate value of each band as related to the XS data set before merging it with the PN data set. By adjusting for the effects of the PN data set's spectral properties when combining the data sets, the spectral quality of the XS data set is mainly preserved (eq. 2-3):

$$BT_{i,j,k} = (XS_{i,j,k} / \sum XS_{i,j,l..n}) \times PN_{i,j} \quad (2-3)$$

where BT is the output image and i and j are pixels of band k.

Principal Components Transformation (PCT)

In order to merge data sets using the Principal Components Transformation model (figure 9), the XS data set is subjected to a Principal Components Transformation (eq. 2-4):

$$PCI_{i,j} = Y_1 X = y_{11} BV_1 + y_{12} BV_2 \dots y_{1n} BV_n \quad (2-4)$$

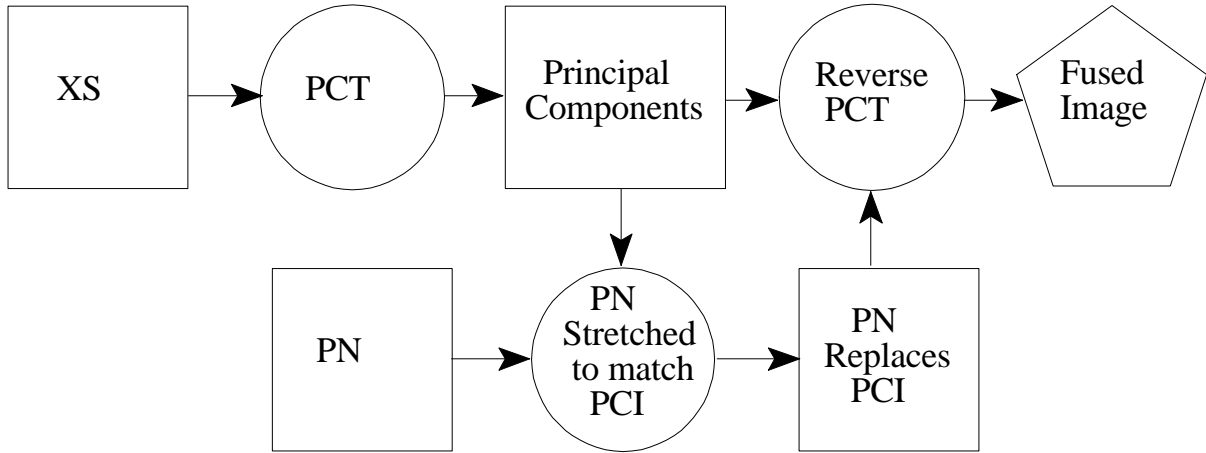


Figure 9: Schematic diagram of the PCT Model.

Where, $PCI_{i,j}$ are the brightness values for the first principal component feature, Y_1 is the first principal component vector, X is the vector representing the digital counts of the spectral bands, and BV are the brightness values. The purpose of the PCT is to maximize the information within the spectral bands that are in common and map that data into the first principal component (PCI). PCI will then, theoretically, contain all the information that is common to all the bands input to the PCT, while spectral information unique to any one input band is mapped to the other principal components (Jensen, 1996, and Chavez, 1991).

For SPOT data, bands 1 and 2 are highly correlated and contain information that is similar to that of the panchromatic data set. When a PCT is implemented, the first principal component contains information related mainly to intensity or brightness, heavily loaded with data from bands 1 and 2. The panchromatic data is then contrast stretched to match the data values of the first principal component. It can then be substituted for the first principal component and an inverse PCT is performed on the combined data sets. This will create an image with fine spatial resolution reasonably correct with respect to brightness values whenever PCI and the panchromatic image are highly correlated (Schott, 1997).

Transforming the data back into RGB space is accomplished using the eigenvectors from the eigenvector matrix (eq. 2-5):

$$BV_{i,j,k} = PCI_{i,j}EV \quad (2-5)$$

where EV are the eigenvectors. This is the inverse function of the original PCT. When using the

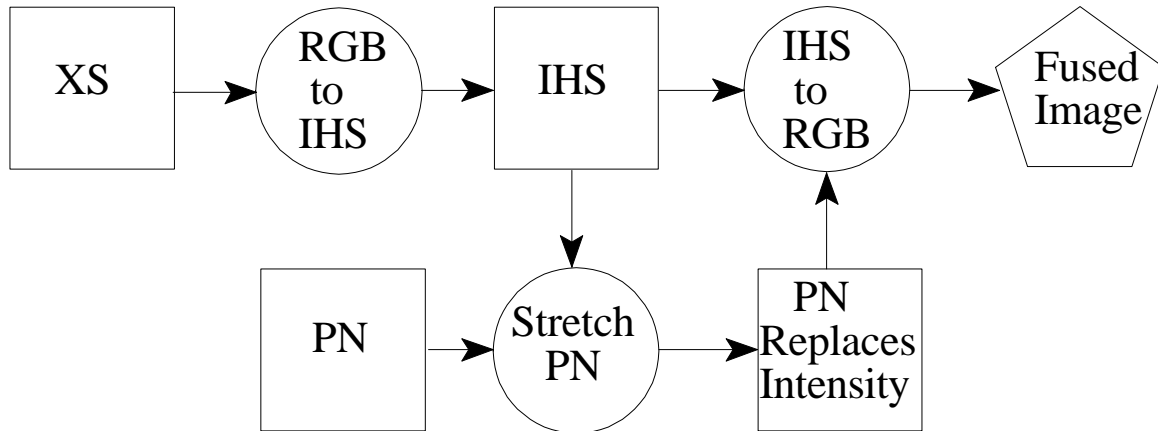


Figure 10: Schematic diagram of the IHS Model.

inverse PCT for data fusion PCI is replaced with the PN data (eq. 2-6):

$$PCT_{i,j,k} = PN_{i,j}EV \quad (2-6)$$

This data conveys the spatial information of the panchromatic data while retaining the majority of the multispectral information.

Intensity-Hue-Saturation Transformation (IHS)

The Intensity-Hue-Saturation model (figure 10) is perhaps the most widely used method of data fusion. It is similar to the PCT model in that the XS data set is transformed into perceptual color space and the PN data is then substituted for the most correlated component--in the IHS transformation case the intensity component (Table 3). The limitation of the IHS transformation is that unlike the PCT model which can be used for a large number of multispectral bands the IHS transformation is limited to three input bands of XS data.

The IHS transformation transforms the data from Red-Green-Blue (RGB) space into their related intensity, hue, and saturation components: where intensity refers to brightness of color, hue

Table 3: Correlation between Panchromatic data, Intensity channel, Principal Component 1, XS 1, and XS 2 for the Laguna Beach Scene.

	Intensity	PC 1	XS 1	XS 2
Panchromatic	0.84471	0.93954	0.91455	0.93362

refers to the dominant or average wavelength of light contributing to a color, and saturation specifies the purity of a color relative to gray. This permits separation of the spatial information into the intensity component from the spectral information, which is split into its related hue and saturation components (Carper et al, 1990). Since intensity is related mainly to the brightness of the spectral responses, the PN data, which is approximately equivalent to the total brightness of the XS bands, can be contrast stretched to match the variance and average of the intensity component and an IHS-to-RGB transformation is performed (Chavez et al, 1991).

To transform the image data from RGB space to color space the data is transformed using the following algorithm (Conrac, 1980):

$$\begin{aligned} R &= (M-R)/(M-m) \\ G &= (M-G)/(M-m) \\ B &= (M-B)/(M-m) \end{aligned}$$

where R,G,B are each in the range of 0 to 1, M is the largest value (either R,G,B), and m is the lowest value (either R,G,B). Then the equations for intensity and saturation are calculated in the range of 0 to 1. The equation for intensity is (eq. 2-7):

$$I = (M+m)/2 \quad (2-7)$$

where I is intensity. The equation for Saturation is (eq. 2-8):

$$\begin{aligned} \text{If } M = m, S &= 0 \\ \text{If } I \leq 0.5, S &= (M-m)/(2-M-m) \\ \text{If } I > 0.5, S &= (M-m)/(2-M-m) \end{aligned} \quad (2-8)$$

where S is saturation. While Hue is placed in the range of 0 to 360 using the equation (eq. 2-9)

$$\begin{aligned} \text{If } M = m, H &= 0 \\ \text{If } R = M, H &= 60(2+b-g) \\ \text{If } G = M, H &= 60(4+r-b) \\ \text{If } B = M, H &= 60(6+g-r) \end{aligned} \quad (2-9)$$

where H is hue, R,G,B are each in the range of 0 to 1, M is the largest values of R,G,B, and m is the least value of R,G,B (Erdas, 1994). Thus, intensity and saturation vary linearly while hue is circular.

To transform the IHS components back into RGB components the following algorithm is used when hue is in the range 0 to 360 and intensity and saturation are in the range 0 to 1 (Conrac, 1980):

$$\begin{aligned}
\text{If } I \leq 0.5, M &= I(I+S) \\
\text{If } I > 0.5, M &= I+S-I(S) \\
m &= 2I-M
\end{aligned}$$

where the stretched panchromatic image is substituted for the intensity (I) component and M is the largest value (either R,G,B) and m is the lowest value (either R,G,B). Then the reverse transformation can occur using the following equation for red (eq. 2-10):

$$\begin{aligned}
\text{If } H < 60, R &= m + (M-m)(H/60) \\
\text{If } H < 180, R &= M \\
\text{If } H < 240, R &= m + (M-m)[(240-H)/60] \\
\text{If } H < 360, R &= m
\end{aligned} \tag{2-10}$$

where H is hue and R is red. The following equation is used for green (eq. 2-11):

$$\begin{aligned}
\text{If } H < 120, G &= m \\
\text{If } H < 180, G &= M \\
\text{If } H < 240, G &= m + (M-m)[(H-120)/60] \\
\text{If } H < 300, G &= M \\
\text{If } H < 360, G &= m + (M-m)[(360-H)/60]
\end{aligned} \tag{2-11}$$

where G is green. The following equation is used for blue (eq. 2-12):

$$\begin{aligned}
\text{If } H < 60, B &= M \\
\text{If } H < 120, B &= m + (M-m)[(120-H)/60] \\
\text{If } H < 240, B &= m \\
\text{If } H < 300, B &= m + (M-m)[(H-240)/60] \\
\text{If } H < 360, B &= M
\end{aligned} \tag{2-12}$$

where B is blue (Erdas, 1994). With the panchromatic data substituted for the intensity component during the transformation from perceptual color space back into spectral space the fine spatial resolution of the PN data is incorporated with the spectral qualities of the XS data maintaining the color balance of the original XS image (Carper et al., 1990).

The five data fusion models introduced in this chapter act upon the PN and XS imagery in diverse and distinct fashions. By applying five data fusion models on imagery of three separate landscapes, the analysis will provide a better understanding of how each model performs on a diversity of landscapes. After each model is applied to the imagery, it will be evaluated statistically, graphically, and for its interpretive potential both for each individual scene and overall.

CHAPTER THREE

METHODS OF EVALUATION

The purpose of data fusion is to improve the high frequency spatial information content of a low frequency multispectral image. A debate stems over how to evaluate the imagery created by a data fusion process. Although the purpose of this thesis is not to propose a standard method for evaluation, it does offer some approaches for judging the effectiveness of a data fusion technique. This chapter will concentrate on the analytical techniques and methodology used to evaluate each data fusion model in this study.

Methods of Evaluation

This study uses statistical, graphical, and photointerpetive methods to evaluate data fusion techniques. The statistical measures are general image statistics of mean and standard deviation, variance/covariance matrices, F test of the variance and mean, correlation matrices, and the spectral root mean square error (SRMSE). The graphical measures are feature space diagrams and spectral profiles. The photointerpetive tests are based on a survey of scientists who are either experts in the field of remote sensing or common users of remotely sensed imagery. These three methods provide statistical, empirical, and qualitative assessments for the determination of a hierarchy of data fusion techniques for discipline related applications.

General Image Statistics

The basic measures of imagery in remote sensing are the mean and standard deviation of each band. These statistics provide analysts with a general understanding of an image. For this study, the mean of each data fusion model was evaluated for its deviation from the mean of the original XS image. The general guideline is that the hybrid images should be within plus or minus one standard deviation of the mean of the original image. The means of all images were then plotted on a three dimensional graph by scene to visualize the similarities and differences.

Statistical Measures

The statistical measures provide both a holistic image analysis and a point-by-point analysis. Variance/covariance and correlation matrices are multivariate image statistics which compare each fused image with the original multispectral data set. Variance/covariance matrices are comparisons of band by band variance/covariance using the equation (eq. 3-1):

$$s^2 = [\sum (BV_{i,j,k} - BV_{Xi})(BV_{i,j,l} - BV_{Xl})]/(n - 1) \quad (3-1),$$

where s^2 represents the variance, $BV_{i,j,k}$ represents the variance of each of the brightness values, and

BV_x represents the mean brightness values of a moving window. To determine the equality of variances and means F tests were performed comparing the data fusion models with the XS image band by band. The F test is based on a probability distribution where the ratio of two variances or means are compared (Davis, 1986). To perform an F test on the means of two samples the differences between variances of the two samples must first be proven to not be significantly different. The correlation matrix standardizes the diagonal terms to equal one, by taking the covariance between two bands and dividing it by the product of their standard deviations as shown in equation (eq. 3-2)(Schowengerdt, 1997):

$$r = s^2_{k,l} / (s^2_{k,k} \times s^2_{l,l})^{1/2} \quad (3-2)$$

where r is the correlation coefficient and s^2 is the covariance of bands k and l . In contrast, the spectral root mean square error (SRMSE) is a point analysis in multispectral space representing the amount of change between the original multispectral pixel and the corresponding output pixels using the following equation (eq. 3-3):

$$SRMSE = \left\{ [(BV_{out(i,j,k)} - BV_{orig(i,j,k)})^2 \times (1/n)] + [(BV_{out(i,j,l)} - BV_{orig(i,j,l)})^2 \times (1/n)] + \dots + [(BV_{out(i,j,n)} - BV_{orig(i,j,n)})^2 \times (1/n)] \right\}^{1/2} \quad (3-3)$$

where BV_{orig} are the original brightness values of the multispectral image, BV_{out} are the resultant brightness values after data fusion, and I and j are pixels of row I and column j of band k, l, \dots, n . A weighting coefficient is applied to each band to compensate for the proportion of error contributed by each band. This coefficient is equal to the quotient of one divided by the number of bands. The total SRMSE can then be evaluated by taking the sum of each individual pixel's SRMSE. The SRMSE measure was developed for this study to isolate an individual pixel's contribution to the overall distortion of each data fusion model. By using an area analysis and a point analysis, the resulting statistics provided a holistic analytical overview of the fused imagery.

Graphical Tests

The graphical tests provide a band combination (area) analysis and a point-by-point analysis. Feature space profiles show a plot of two bands in multispectral space. For this study, bands 2 and 3 are plotted against each other to analyze the spectral integrity in the near infrared and the red bands, which are very important for vegetation analysis. Spectral profiles, correspond to the SRMSE, in that they are a point analysis. Spectral profiles show the brightness values (BV) for all three bands at a given point. Again, by using area and point graphical analysis the results are complementary and more reliable for evaluation.

Photointerpetive Measures

The photointerpetive analysis allows scientists who use remotely sensed data to evaluate the

quality of the fused images as compared with the original multispectral and panchromatic images. The scientists chosen, represent each of the disciplines discussed above: environmental, planning, agriculture, forestry, geology, and cartography. Each scientist was asked to evaluate the images for spatial resolution, spectral quality, and interpretability (Appendix B).

The scientists evaluated each criterion based on a scale of 0 to 100. Spatial resolution is based on a comparison of the fused images with the multispectral and panchromatic images, with 0 being a resolution equal to the original multispectral imagery and 100 being a resolution equal to the panchromatic imagery. Spectral quality is an evaluation of the fused images as compared with the original multispectral image, with a score of 0 being very poor and a score of 100 being equal to the original multispectral image. Interpretability is based on the photographic quality of the resulting fused images. For interpretability a score of 0 means a decrease in photointerpretive potential, a score of 50 means the fused image is equivalent to the original panchromatic or multispectral imagery for interpretability, and a score of 100 means an increase in photointerpretive potential over the panchromatic and multispectral imagery as stand alone data sets.

An analysis of variance (ANOVA) two way without replication was performed on the resulting data to determine whether the variance of the ten analysts was a product of the five data fusion models (samples) or the three scenes (treatments). Each of the three evaluation criteria, spatial resolution, spectral quality, and photointerpretive potential were evaluated separately. The average response for each of the ten analysts for each data fusion model per scene was analyzed using each scene as a treatment. The ANOVA provided information concerning the two main sources of variation per criterion; those influenced by differences between scenes and those influenced by differing scenes.

After the three methods of evaluation had been completed, the results were compiled and analyzed for trends. The analysis of these trends resulted in a table that lists the discipline related applications for which each data fusion model could be applicable. The table is based on the criteria listed in Chapter One. Each model was given a rating based on their performance for each of the discipline related requirements as related to spatial and spectral resolution. Where both spatial and spectral resolution were given equal weight within the ranking. This table will be a look-up table for analysts interested in increasing spatial resolution and at what cost spectral integrity will be affected. The following chapters present the results and conclusions as related to the tests of the five data fusion techniques on the three scenes.

CHAPTER FOUR

RESULTS AND ANALYSIS

This chapter describes the examination of each of the data fusion techniques using the statistical, graphical, and photointerpretive techniques outlined in the previous chapters. Figures 11 through 25 represent the resultant hybrid imagery after being processed. Each image was contrast stretched for display purposes for reasons that will be noted during analysis.

Figure 11: HPF model for Blacksburg, Virginia area.

Figure 12: MLT model for Blacksburg, Virginia area.

Figure 13: BT model for Blacksburg, Virginia area.

Figure 14: PCT model for Blacksburg, Virginia area.

Figure 15: IHS model for Blacksburg, Virginia area.

Figure 16: HPF model for Laguna Beach, California area.

Figure 17: MLT model for Laguna Beach, California area.

Figure 18: BT model for Laguna Beach, California area.

Figure 19: PCT model for Laguna Beach, California area.

Figure 20: IHS model for Laguna Beach, California area.

Figure 21: HPF model for Seattle, Washington area.

Figure 22: MLT model for Seattle, Washington area.

Figure 23: BT model for Seattle, Washington area.

Figure 24: PCT model for Seattle, Washington area.

Figure 25: IHS model for Seattle, Washington area.

Table 4: Means and Standard Deviations for the three scenes' multispectral data and the resultant data fusion models.

Blacksburg	Mean	SD	Laguna Beach	Mean	SD	Seattle	Mean	SD
XS1	59.45	9.74	XS1	44.68	10.64	XS1	66.57	16.50
XS2	47.30	10.45	XS2	39.65	13.49	XS2	44.96	17.30
XS3	82.14	21.20	XS3	44.86	17.07	XS3	59.70	32.48
HPF1	50.01	13.30	HPF1	46.51	18.13	HPF1	57.82	26.22
HPF2	43.94	13.44	HPF2	44.00	19.27	HPF2	47.06	26.52
HPF3	61.36	16.89	HPF3	46.60	19.71	HPF3	54.45	29.40
MLT1	7.88	5.66	MLT1	11.93	9.73	MLT1	9.67	11.17
MLT2	7.84	5.73	MLT2	11.30	9.78	MLT2	7.58	9.62
MLT3	17.07	8.82	MLT3	16.17	11.30	MLT3	14.78	12.16
BT1	19.65	9.61	BT1	33.38	16.07	BT1	29.35	17.88
BT2	20.11	10.00	BT2	31.41	17.48	BT2	25.79	19.05
BT3	28.70	11.28	BT3	43.20	18.50	BT3	35.41	22.10
PCT1	36.34	10.75	PCT1	37.01	10.13	PCT1	60.46	19.36
PCT2	43.15	12.51	PCT2	30.00	12.92	PCT2	38.74	20.33
PCT3	45.06	9.06	PCT3	32.75	12.62	PCT3	44.11	20.90
IHS1	37.55	14.22	IHS1	48.78	19.59	IHS1	49.88	21.77
IHS2	39.39	15.39	IHS2	45.09	21.84	IHS2	35.66	20.29
IHS3	88.96	20.86	IHS3	59.27	23.17	IHS3	67.42	32.77

General image statistics (table 4 and figures 26, 27, and 28) of mean and standard deviation show the general trends of each data fusion model. The IHS model maintains the statistical qualities of the XS data within \pm one standard deviation of the mean for all three bands for all three scenes. Similarly, the HPF model is within \pm one standard deviation of the XS mean with band 3 having significantly decreased brightness values in all three scenes. The PCT model tends to decrease the mean for all bands, but with the exception of the Blacksburg scene, the mean for all the data sets is within \pm one standard deviation of the original data. The BT model maintains the mean within \pm

Blacksburg Mean Brightness Values

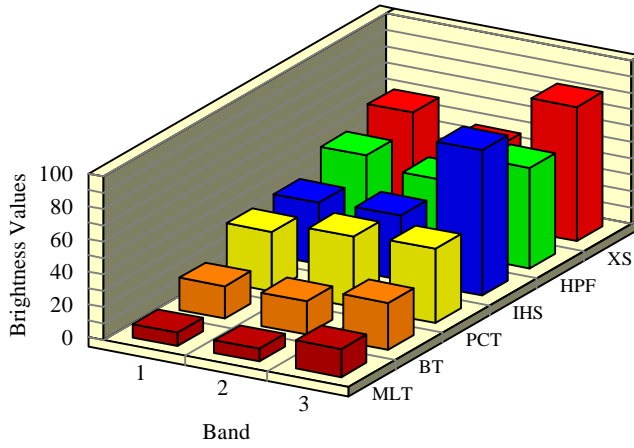


Figure 26: Blacksburg mean brightness values for original XS image and the five data fusion models.

Laguna Beach Mean Brightness Values

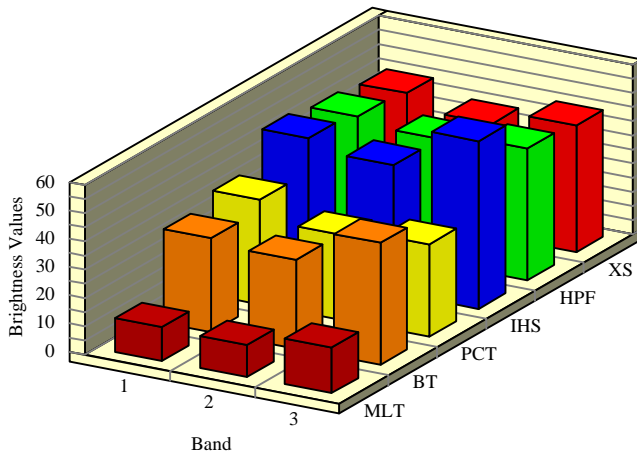


Figure 27: Laguna Beach mean brightness values for original XS image and the five data fusion models.

Seattle Mean Brightness Values

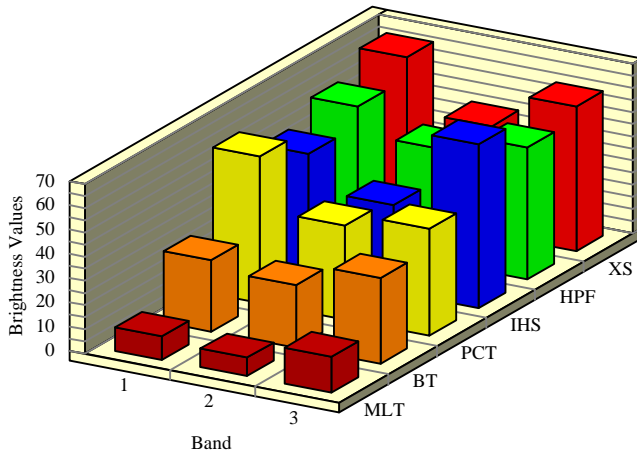


Figure 28: Seattle mean brightness values for original XS image and the five data fusion models.

one standard deviation for the Laguna Beach scene only and decreases brightness values significantly for the other two scenes. The MLT model decreases the average brightness values below tolerance on all scenes. Although means and standard deviations do not explain the factors that are affecting the spectral deviations, they do provide an overview of the general trends that will be brought out in later analysis.

Statistical Measures

Tables 5 through 10 present variance/covariance and correlation matrices for each of the three scenes. Typically, bands 1 and 2 are highly correlated in the original XS data, due to their imaging range within the visible portion of the electromagnetic spectrum. Band 3 has a lower correlation with the three bands due to its imaging range within the near infrared region of the electromagnetic spectrum. The variance/covariance matrices and to a greater degree the correlation matrices of the data fusion models should be similar in their values as compared with the XS data. The goal then is to maintain the variance/covariance of each band and the correlations among and within channels.

The variance/covariance matrices reinforce the general statistics. The IHS model tends to increase variances, yet is most similar to the original XS data for both the Blacksburg and Seattle scenes specifically within Band 3. The HPF model increases variances greatly but maintains the general trend of band 3 having the greatest variance. The PCT model has similar variances for band 1 and 2 but decreases the variance of band 3 to below the variance relationships of the original XS data. The BT model has similar variances within band 1 and 2 and similar to the PCT tends to decrease the variance of band 3. Again the MLT model decreases the brightness values resulting in lower variances within all three channels.

The correlation matrices show the ability of the data fusion models to maintain correlations among channels. For the Blacksburg scene, the IHS model maintains the overall correlation among channels when compared with the XS correlations, followed by the PCT model and to a lesser degree the BT models. Similarly for the Laguna Beach, scene the IHS model keeps the general correlation with the BT model and PCT model, maintaining similar correlations with the former being higher and the later being lower. The Seattle scene shows the same trend of the IHS model maintaining correlation followed by the BT model. These relationships show that the IHS model maintains the best overall correlation when compared with the original XS data. Following close behind are the BT model and the PCT model.

When the correlation between the data fusion models and the original XS data is compared the correlation should optimally be one. The Blacksburg scene reveals that the MLT model maintains correlation between band 1 at the 90 percent level. The PCT model maintains the correlation between band 2 at the 90 percent level. The IHS and BT model keep an 80 percent correlation among all three bands of the XS data set. For the Laguna Beach scene the trend is similar with the MLT model having a 90 percent correlation with bands 1 and 2, the IHS and BT model having a 90 percent correlation with bands 2 and 3, and the PCT model having a 90 percent correlation with band 2 only. The Seattle scene shows the MLT model having a 90 percent

Table 5: Variance/covariance matrix for the Blacksburg data fusion models (row labels are the transpose of column labels).

<u>XS1</u>	<u>XS2</u>	<u>XS3</u>	<u>HPF1</u>	<u>HPF2</u>	<u>HPF3</u>	<u>MLT1</u>	<u>MLT2</u>	<u>MLT3</u>	<u>BT1</u>	<u>BT2</u>	<u>BT3</u>	<u>PCT1</u>	<u>PCT2</u>	<u>PCT3</u>	<u>IHS1</u>	<u>IHS2</u>	<u>IHS3</u>
94.97	96.96	91.69	94.91	96.08	93.48	50.09	50.92	61.53	78.98	83.96	62.47	93.29	102.03	50.48	111.16	123.36	108.76
96.96	110.11	69.30	95.45	102.16	81.80	50.11	53.79	55.99	80.29	92.90	53.10	100.50	122.07	43.45	115.53	141.08	91.01
91.69	69.30	449.17	112.70	101.59	291.53	53.34	46.92	161.78	51.43	43.76	207.16	4.02	-8.85	144.82	30.05	25.39	377.43
94.91	95.45	112.70	176.64	177.13	185.77	62.29	61.48	84.74	109.4	110.10	102.74	99.82	106.28	90.93	149.21	156.20	180.27
96.08	102.16	101.59	177.13	180.53	180.19	62.50	63.11	82.15	110.39	114.80	98.20	103.65	116.49	87.58	151.64	165.29	171.54
93.48	81.80	291.53	185.77	180.19	285.12	64.15	59.71	135.02	95.96	90.24	175.19	55.43	51.06	138.23	108.89	107.45	314.70
50.09	50.11	53.34	62.29	62.50	64.15	32.05	31.90	40.05	50.26	51.47	43.03	51.16	54.40	37.41	66.49	71.04	72.35
50.92	53.79	46.92	61.48	63.11	59.71	31.90	32.78	38.14	49.99	53.34	39.43	53.22	59.76	34.49	66.80	74.91	65.45
61.53	55.99	161.78	84.74	82.15	135.06	40.05	38.14	77.72	56.85	55.25	95.42	40.73	40.03	74.17	65.69	67.34	169.76
78.98	80.29	51.43	109.48	110.39	95.96	50.26	49.99	56.85	92.32	93.08	66.02	92.44	98.05	62.24	131.54	137.13	114.64
83.96	92.90	43.76	110.10	114.80	90.24	51.47	53.34	55.25	93.08	99.91	60.69	98.92	113.72	57.38	133.67	149.53	103.94
62.47	53.10	207.16	102.74	98.20	175.19	43.03	39.43	95.42	66.02	60.69	127.26	35.41	30.79	99.61	76.64	73.15	232.00
93.29	100.50	4.02	99.82	103.65	55.43	51.16	53.22	40.73	92.44	98.92	35.41	115.52	128.20	36.50	140.06	154.06	58.34
102.03	122.07	-8.85	106.28	116.49	51.06	54.40	59.76	40.03	98.05	113.72	30.79	128.20	156.38	32.74	150.08	180.45	48.90
50.48	43.45	144.82	90.93	87.58	138.23	37.41	34.49	74.17	62.24	57.38	99.61	36.50	32.74	82.06	75.83	72.24	179.96
111.16	115.53	30.05	149.21	151.64	108.89	66.49	66.80	65.69	131.54	133.67	76.64	140.06	150.08	75.83	202.07	210.03	140.57
123.36	141.08	25.39	156.20	165.29	107.45	71.04	74.91	67.34	137.13	149.53	73.15	154.06	180.45	72.24	210.03	236.77	131.59
108.76	91.01	377.43	180.27	171.54	314.70	72.35	65.45	169.76	114.64	103.94	232.00	58.34	48.90	179.96	140.57	131.59	434.96

Table 6: Correlation matrix for the Blacksburg data fusion models (row labels are the transpose of column labels).

<u>XS1</u>	<u>XS2</u>	<u>XS3</u>	<u>HPF1</u>	<u>HPF2</u>	<u>HPF3</u>	<u>MLT1</u>	<u>MLT2</u>	<u>MLT3</u>	<u>BT1</u>	<u>BT2</u>	<u>BT3</u>	<u>PCT1</u>	<u>PCT2</u>	<u>PCT3</u>	<u>IHS1</u>	<u>IHS2</u>	<u>IHS3</u>
1	0.94	0.44	0.73	0.73	0.56	0.90	0.91	0.71	0.84	0.86	0.56	0.89	0.83	0.57	0.80	0.82	0.53
0.94	1	0.31	0.68	0.72	0.46	0.84	0.89	0.60	0.79	0.88	0.44	0.89	0.93	0.45	0.77	0.87	0.41
0.44	0.31	1	0.40	0.35	0.81	0.44	0.38	0.86	0.25	0.20	0.86	0.01	-0.03	0.75	0.09	0.07	0.85
0.73	0.68	0.40	1	0.99	0.82	0.82	0.80	0.72	0.85	0.82	0.68	0.69	0.63	0.75	0.78	0.76	0.65
0.73	0.72	0.35	0.99	1	0.79	0.82	0.82	0.69	0.85	0.85	0.64	0.71	0.69	0.71	0.79	0.79	0.61
0.56	0.46	0.81	0.82	0.79	1	0.67	0.61	0.90	0.59	0.53	0.91	0.30	0.24	0.90	0.45	0.41	0.89
0.90	0.84	0.44	0.82	0.82	0.67	1	0.98	0.80	0.92	0.90	0.67	0.84	0.76	0.72	0.82	0.81	0.61
0.91	0.89	0.38	0.80	0.82	0.61	0.98	1	0.75	0.90	0.93	0.61	0.86	0.83	0.66	0.82	0.85	0.54
0.71	0.60	0.86	0.72	0.69	0.90	0.80	0.75	1	0.67	0.62	0.95	0.42	0.36	0.92	0.52	0.49	0.92
0.84	0.79	0.25	0.85	0.85	0.59	0.92	0.90	0.67	1	0.96	0.60	0.89	0.81	0.71	0.96	0.92	0.57
0.86	0.88	0.20	0.82	0.85	0.53	0.90	0.93	0.62	0.96	1	0.53	0.92	0.90	0.63	0.94	0.97	0.49
0.56	0.44	0.86	0.68	0.64	0.91	0.67	0.61	0.95	0.60	0.53	1	0.29	0.21	0.97	0.47	0.42	0.98
0.89	0.89	0.01	0.69	0.71	0.30	0.84	0.86	0.42	0.89	0.92	0.29	1	0.95	0.37	0.91	0.93	0.26
0.83	0.93	-0.03	0.63	0.69	0.24	0.76	0.83	0.36	0.81	0.90	0.21	0.95	1	0.28	0.84	0.93	0.18
0.57	0.45	0.75	0.75	0.71	0.90	0.72	0.66	0.92	0.71	0.63	0.97	0.37	0.28	1	0.58	0.51	0.95
0.80	0.77	0.09	0.78	0.79	0.45	0.82	0.82	0.52	0.96	0.94	0.47	0.91	0.84	0.58	1	0.96	0.47
0.82	0.87	0.07	0.76	0.79	0.41	0.81	0.85	0.49	0.92	0.97	0.42	0.93	0.93	0.51	0.96	1	0.41
0.53	0.41	0.85	0.65	0.61	0.89	0.61	0.54	0.92	0.57	0.49	0.98	0.26	0.18	0.95	0.47	0.41	1

Table 7: Variance/covariance matrix for the Laguna Beach data fusion models (row labels are the transpose of column labels).

<u>XS1</u>	<u>XS2</u>	<u>XS3</u>	<u>HPF1</u>	<u>HPF2</u>	<u>HPF3</u>	<u>MLT1</u>	<u>MLT2</u>	<u>MLT3</u>	<u>BT1</u>	<u>BT2</u>	<u>BT3</u>	<u>PCT1</u>	<u>PCT2</u>	<u>PCT3</u>	<u>IHS1</u>	<u>IHS2</u>	<u>IHS3</u>
113.21	140.47	131.60	142.56	156.19	151.77	97.84	97.07	108.12	149.95	168.46	162.31	96.61	119.22	104.76	182.44	209.51	198.94
140.47	181.83	168.50	181.81	202.48	195.84	123.02	124.03	137.79	189.04	220.15	211.73	120.56	156.29	136.31	231.17	275.18	260.51
131.60	168.50	291.23	166.86	185.31	246.68	108.53	107.72	162.75	126.37	166.41	286.58	72.66	94.02	195.89	155.04	207.28	359.37
142.56	181.81	166.86	328.73	348.26	340.82	143.92	142.03	160.09	251.25	269.92	264.21	149.86	191.02	178.71	299.25	330.07	318.20
156.19	202.48	185.31	348.26	371.44	362.83	156.49	155.49	174.91	270.78	295.75	288.91	161.83	209.55	194.47	323.60	362.88	348.97
151.77	195.84	246.68	340.82	362.83	388.34	149.27	147.36	187.41	239.47	268.90	326.34	137.90	178.44	224.27	285.57	328.97	398.41
97.84	123.02	108.53	143.92	156.49	149.27	94.73	94.75	103.45	145.65	160.86	148.62	91.23	114.52	97.84	170.76	194.66	176.63
97.07	124.03	107.72	142.03	155.49	147.36	94.75	95.73	103.88	144.62	161.96	147.93	90.52	115.60	97.14	168.83	195.62	175.25
108.12	137.79	162.75	160.09	174.91	187.41	103.45	103.88	127.66	146.50	168.96	195.28	88.72	113.17	131.37	169.73	202.98	234.47
149.95	189.04	126.37	251.25	270.78	239.47	145.65	144.62	146.50	258.15	274.42	219.37	160.75	202.50	143.86	308.92	337.38	261.78
168.46	220.15	166.41	269.92	295.75	268.90	160.86	161.96	168.96	274.42	305.40	260.22	170.60	222.58	169.90	331.12	377.97	314.33
162.31	211.73	286.58	264.21	288.91	326.34	148.62	147.93	195.28	219.37	260.22	341.97	128.31	168.59	231.61	267.25	323.21	424.40
96.61	120.56	72.662	149.86	161.83	137.90	91.23	90.52	88.72	160.75	170.60	128.31	102.51	127.68	82.09	193.70	210.76	153.55
119.22	156.29	94.025	191.02	209.55	178.44	114.52	115.60	113.17	202.50	222.58	168.59	127.68	166.82	107.73	245.07	276.34	202.78
104.76	136.31	195.89	178.71	194.47	224.27	97.84	97.14	131.37	143.86	169.90	231.61	82.09	107.73	159.30	173.29	209.35	285.98
182.44	231.17	155.04	299.25	323.60	285.57	170.76	168.83	169.73	308.92	331.12	267.25	193.70	245.07	173.29	383.84	418.02	329.94
209.51	275.18	207.28	330.07	362.88	328.97	194.66	195.62	202.98	337.38	377.97	323.21	210.76	276.34	209.35	418.02	476.80	399.21
198.94	260.51	359.37	318.20	348.97	398.41	176.63	175.25	234.47	261.78	314.33	424.40	153.55	202.78	285.98	329.94	399.21	536.90

Table 8: Correlation matrix for the Laguna Beach data fusion models (row labels are the transpose of column labels).

<u>XS1</u>	<u>XS2</u>	<u>XS3</u>	<u>HPF1</u>	<u>HPF2</u>	<u>HPF3</u>	<u>MLT1</u>	<u>MLT2</u>	<u>MLT3</u>	<u>BT1</u>	<u>BT2</u>	<u>BT3</u>	<u>PCT1</u>	<u>PCT2</u>	<u>PCT3</u>	<u>IHS1</u>	<u>IHS2</u>	<u>IHS3</u>
1	0.97	0.72	0.73	0.76	0.72	0.94	0.93	0.89	0.87	0.90	0.82	0.89	0.86	0.78	0.87	0.90	0.80
0.97	1	0.73	0.74	0.77	0.73	0.93	0.94	0.90	0.87	0.93	0.84	0.88	0.89	0.80	0.87	0.93	0.83
0.72	0.73	1	0.53	0.56	0.73	0.65	0.64	0.84	0.46	0.55	0.90	0.42	0.42	0.90	0.46	0.55	0.90
0.73	0.74	0.53	1	0.99	0.95	0.81	0.80	0.78	0.86	0.85	0.78	0.81	0.81	0.78	0.84	0.83	0.75
0.76	0.77	0.56	0.99	1	0.95	0.83	0.82	0.80	0.87	0.87	0.81	0.82	0.84	0.79	0.85	0.86	0.78
0.72	0.73	0.73	0.95	0.95	1	0.77	0.76	0.84	0.75	0.78	0.89	0.69	0.70	0.90	0.73	0.76	0.87
0.94	0.93	0.65	0.81	0.83	0.77	1	0.99	0.94	0.93	0.94	0.82	0.92	0.91	0.79	0.89	0.91	0.78
0.93	0.94	0.64	0.80	0.82	0.76	0.99	1	0.93	0.91	0.94	0.81	0.91	0.91	0.78	0.88	0.91	0.77
0.89	0.90	0.84	0.78	0.80	0.84	0.94	0.93	1	0.80	0.85	0.93	0.77	0.77	0.92	0.76	0.82	0.89
0.87	0.87	0.46	0.86	0.87	0.75	0.93	0.91	0.80	1	0.97	0.73	0.98	0.97	0.70	0.98	0.96	0.70
0.90	0.93	0.55	0.85	0.87	0.78	0.94	0.94	0.85	0.97	1	0.80	0.96	0.98	0.77	0.96	0.99	0.77
0.82	0.84	0.90	0.78	0.81	0.89	0.82	0.81	0.93	0.73	0.80	1	0.68	0.70	0.99	0.73	0.80	0.99
0.89	0.88	0.42	0.81	0.82	0.69	0.92	0.91	0.77	0.98	0.96	0.68	1	0.97	0.64	0.97	0.95	0.65
0.86	0.89	0.42	0.81	0.84	0.70	0.91	0.91	0.77	0.97	0.98	0.70	0.97	1	0.66	0.96	0.97	0.67
0.78	0.80	0.90	0.78	0.79	0.90	0.79	0.78	0.92	0.70	0.77	0.99	0.64	0.66	1	0.70	0.75	0.97
0.87	0.87	0.46	0.84	0.85	0.73	0.89	0.88	0.76	0.98	0.96	0.73	0.97	0.96	0.70	1	0.97	0.72
0.90	0.93	0.55	0.83	0.86	0.76	0.91	0.91	0.82	0.96	0.99	0.80	0.95	0.97	0.75	0.97	1	0.78
0.80	0.83	0.90	0.75	0.78	0.87	0.78	0.77	0.89	0.70	0.77	0.99	0.65	0.67	0.97	0.72	0.78	1

Table 9: Variance/covariance matrix for the Seattle data fusion models (row labels are the transpose of column labels).

<u>XS1</u>	<u>XS2</u>	<u>XS3</u>	<u>HPF1</u>	<u>HPF2</u>	<u>HPF3</u>	<u>MLT1</u>	<u>MLT2</u>	<u>MLT3</u>	<u>BT1</u>	<u>BT2</u>	<u>BT3</u>	<u>PCT1</u>	<u>PCT2</u>	<u>PCT3</u>	<u>IHS1</u>	<u>IHS2</u>	<u>IHS3</u>
272.22	282.01	254.40	305.50	312.99	301.31	166.01	141.62	160.86	236.45	277.09	261.77	281.63	292.03	281.09	315.57	305.36	321.12
282.01	299.45	254.33	311.19	322.36	301.88	169.82	146.30	162.80	245.67	293.55	268.86	294.53	312.63	289.39	335.51	329.69	333.77
254.40	254.33	1054.78	265.70	266.93	668.03	126.06	102.28	310.73	11.41	97.581	637.76	26.45	21.90	441.83	146.41	185.62	995.22
305.50	311.19	265.70	687.27	694.06	674.09	228.43	190.18	217.58	374.73	399.65	373.72	374.61	382.26	453.06	433.51	395.05	410.19
312.99	322.36	266.93	694.06	703.21	678.42	233.09	194.83	220.84	382.92	411.48	379.74	384.53	395.91	460.86	446.70	410.14	418.54
301.31	301.88	668.03	674.09	678.42	864.33	213.58	174.90	296.72	268.56	316.42	565.90	253.27	253.32	539.76	354.70	340.55	750.68
166.01	169.82	126.06	228.43	233.09	213.58	124.74	106.95	113.20	176.74	195.50	161.73	191.79	196.67	196.96	204.79	193.30	172.86
141.62	146.30	102.28	190.18	194.83	174.90	106.95	92.49	96.02	150.22	167.54	133.93	164.24	169.87	164.57	174.06	165.84	141.56
160.86	162.80	310.73	217.58	220.84	296.72	113.20	96.02	147.82	121.29	150.59	249.57	130.93	132.71	231.50	164.52	164.32	331.91
236.45	245.67	11.41	374.73	382.92	268.56	176.74	150.22	121.29	319.60	332.91	171.68	334.82	346.57	277.41	356.16	322.12	131.98
277.09	293.55	97.58	399.65	411.48	316.42	195.50	167.54	150.59	332.91	362.74	228.85	358.99	377.66	319.41	392.88	367.60	222.22
261.77	268.86	637.76	373.72	379.74	565.90	161.73	133.93	249.57	171.68	228.85	488.62	181.45	187.21	422.37	279.64	281.82	695.96
281.63	294.53	26.45	374.61	384.53	253.27	191.79	164.24	130.93	334.82	358.99	181.45	374.96	390.20	278.84	393.73	362.90	151.46
292.03	312.63	21.90	382.26	395.91	253.32	196.67	169.87	132.71	346.57	377.66	187.21	390.20	413.39	287.59	415.77	388.87	160.83
281.09	289.39	441.83	453.06	460.86	539.76	196.96	164.57	231.50	277.41	319.41	422.37	278.84	287.59	437.00	358.15	341.79	539.12
315.57	335.51	146.41	433.51	446.70	354.70	204.79	174.06	164.52	356.16	392.88	279.64	393.73	415.77	358.15	473.89	434.46	324.30
305.36	329.69	185.62	395.05	410.14	340.55	193.30	165.84	164.32	322.12	367.60	281.82	362.90	388.87	341.79	434.46	411.48	337.92
321.12	333.77	995.22	410.19	418.54	750.68	172.86	141.56	331.91	131.98	222.22	695.96	151.46	160.83	539.12	324.30	337.92	1074.19

Table 10: Correlation matrix for the Seattle data fusion models (row labels are the transpose of column labels).

<u>XS1</u>	<u>XS2</u>	<u>XS3</u>	<u>HPF1</u>	<u>HPF2</u>	<u>HPF3</u>	<u>MLT1</u>	<u>MLT2</u>	<u>MLT3</u>	<u>BT1</u>	<u>BT2</u>	<u>BT3</u>	<u>PCT1</u>	<u>PCT2</u>	<u>PCT3</u>	<u>IHS1</u>	<u>IHS2</u>	<u>IHS3</u>
1	0.98	0.47	0.70	0.71	0.62	0.90	0.89	0.80	0.80	0.88	0.71	0.88	0.87	0.81	0.87	0.91	0.59
0.98	1	0.45	0.68	0.70	0.59	0.87	0.87	0.77	0.79	0.89	0.70	0.87	0.88	0.80	0.89	0.93	0.58
0.47	0.45	1	0.31	0.30	0.69	0.34	0.32	0.78	0.01	0.15	0.88	0.04	0.03	0.65	0.20	0.28	0.93
0.70	0.68	0.31	1	0.99	0.87	0.78	0.75	0.68	0.79	0.80	0.64	0.73	0.71	0.82	0.75	0.74	0.47
0.71	0.70	0.30	0.99	1	0.87	0.78	0.76	0.68	0.80	0.81	0.64	0.74	0.73	0.83	0.77	0.76	0.48
0.62	0.59	0.69	0.87	0.87	1	0.65	0.61	0.83	0.51	0.56	0.87	0.44	0.42	0.87	0.55	0.57	0.77
0.90	0.87	0.34	0.78	0.78	0.65	1	0.99	0.83	0.88	0.91	0.65	0.88	0.86	0.84	0.84	0.85	0.47
0.89	0.87	0.32	0.75	0.76	0.61	0.99	1	0.82	0.87	0.91	0.62	0.88	0.86	0.81	0.83	0.85	0.44
0.80	0.77	0.78	0.68	0.68	0.83	0.83	0.82	1	0.55	0.65	0.92	0.55	0.53	0.91	0.62	0.66	0.83
0.80	0.79	0.01	0.79	0.80	0.51	0.88	0.87	0.55	1	0.97	0.43	0.96	0.95	0.74	0.91	0.88	0.22
0.88	0.89	0.15	0.80	0.81	0.56	0.91	0.91	0.65	0.97	1	0.546	0.97	0.97	0.80	0.94	0.95	0.35
0.71	0.70	0.88	0.64	0.64	0.87	0.65	0.62	0.92	0.43	0.54	1	0.42	0.41	0.91	0.58	0.62	0.96
0.88	0.87	0.04	0.73	0.74	0.44	0.88	0.88	0.55	0.96	0.97	0.42	1	0.99	0.68	0.93	0.92	0.23
0.87	0.88	0.03	0.71	0.73	0.42	0.86	0.86	0.53	0.95	0.97	0.41	0.99	1	0.67	0.93	0.94	0.24
0.81	0.80	0.65	0.82	0.83	0.87	0.84	0.81	0.91	0.74	0.80	0.91	0.68	0.67	1	0.78	0.80	0.78
0.87	0.89	0.20	0.75	0.77	0.55	0.84	0.83	0.62	0.91	0.94	0.58	0.93	0.93	0.78	1	0.98	0.45
0.91	0.93	0.28	0.74	0.76	0.57	0.85	0.85	0.66	0.88	0.95	0.62	0.92	0.94	0.80	0.98	1	0.50
0.59	0.58	0.93	0.47	0.48	0.77	0.47	0.44	0.83	0.22	0.35	0.96	0.23	0.24	0.78	0.45	0.50	1

Table 11: Spectral Root Mean Square Errors for the Blacksburg data fusion models.

Contribution	HPF	MLT	BT	PCT	IHS
Urban	3.79	50.11	33.49	12.07	9.75
Urban	15.21	59.94	42.81	19.33	7.44
Urban	101.38	49.57	41.23	21.31	10.08
Urban	11.94	50.07	34.54	16.06	14.62
Urban	47.78	63.83	48.92	22.20	17.29
Urban	21.34	57.81	46.24	26.31	13.40
Soil	16.46	62.38	46.65	26.09	11.90
Agriculture	31.44	77.86	70.03	62.81	37.08
Agriculture	35.83	76.67	68.13	60.04	40.77
Agriculture	21.63	63.36	48.95	42.22	18.57
Agriculture	33.17	77.43	70.37	62.66	41.45
Agriculture	30.01	71.94	64.36	54.70	33.73
Agriculture	26.27	67.02	55.00	48.27	20.31
Agriculture	25.94	68.13	60.06	49.53	30.56
Agriculture	24.56	63.58	52.72	44.35	22.88
Forest	20.46	52.69	41.81	22.61	14.36
Forest	9.11	47.02	37.01	18.49	14.55
Forest	14.27	51.37	40.75	21.65	15.19
Forest	5.51	47.40	34.47	17.22	12.33
Shadow	7.59	53.77	48.20	30.90	21.57
SRMSE	26.51	63.79	51.88	35.73	21.46

correlation with the XS's band 1 only and the IHS model again maintains a 90 percent correlation with bands 2 and 3. By comparing the correlation of the data fusion models with the original XS data, it can be seen that the best model for band 1 preservation is the MLT model while the IHS model is the best overall for whole image correlation preservation.

After initial comparisons of the variance/covariance matrices and means of the three scene's data fusion models and XS image, F tests were performed to evaluate the equality of the variances and means of each band of each model as compared with the original XS image for each scene. The F tests for the 99th percentile ($\alpha = 0.01$) have a critical value of 1.70 (Davis, 1986). For the Blacksburg scene: the HPF model was not significantly different from the XS data's variance and means for bands 2 and 3; the BT and PCT model were statistically similar to the XS data for bands 1 and 2; while the IHS model retained the qualities of the variance and means for band 3. For the Laguna Beach scene: the HPF model was statistically similar to the XS image for band 3; the MLT model was similar to the XS image for band 1; the BT model was not significantly different when

Table 12: Spectral Root Mean Square Errors for the Laguna Beach data fusion models.

Contribution	HPF	MLT	BT	PCT	IHS
Urban	4.36	29.08	4.51	5.07	13.77
Urban	7.87	32.40	3.00	7.44	19.02
Agriculture	20.62	51.72	34.63	34.55	29.20
Agriculture	12.06	43.82	25.28	29.09	16.68
Agriculture	10.34	28.97	11.34	10.54	9.33
Agriculture	12.83	40.88	24.22	26.46	16.05
Agriculture	7.59	34.77	20.04	19.68	14.39
Agriculture	6.88	28.25	5.48	5.48	14.17
Soil	6.45	35.29	5.72	22.78	14.20
Soil	20.93	44.03	22.18	24.43	6.98
Soil	2.38	27.38	10.08	7.44	4.12
Soil	24.01	28.79	12.97	6.78	30.41
Soil	3.83	33.02	4.36	10.13	23.73
Soil	4.36	29.72	7.85	8.16	12.30
Soil	4.16	26.60	13.74	10.13	7.14
Soil	8.27	31.52	6.66	12.25	28.34
Water	6.24	17.52	8.10	0.00	7.33
Water	5.29	20.53	7.96	1.73	3.74
Fire Scar	3.70	19.84	11.58	5.07	7.07
Fire Scar	14.94	30.40	4.43	3.70	22.11
SRMSE	9.85	33.40	12.85	13.21	15.79

compared to the XS data for bands 2 and 3; and, the PCT model retained the qualities of variance and means for bands 1 and 2. For the Seattle scene: the HPF model was statistically similar to band 3 of the XS image; the BT model maintained the variances and means for bands 1 and 2 when compared with the XS's statistics; the PCT model was similar for bands 1 and 2; while the IHS model was not significantly different for bands 2 and 3 when compared with the XS data. At the 95th percentile ($\alpha = 0.05$) the critical value was 1.46. Similar results were seen at this level with the noted exceptions of for the Blacksburg scene bands 2 and 3 of the HPF model were not similar to the original XS data and for the Laguna Beach scene band 2 was not statistically equivalent to the XS data (See Appendix A).

By using the Spectral Root Mean Square Error the overall error is seen as well as which landscape feature provides the highest amount of error for each data fusion model. Tables 11, 12, and 13 present the SRMSE for each band along with each landscape features general contribution. For the Blacksburg scene, the IHS model had the lowest error of 21.46 brightness value deviations

Table 13: Spectral Root Mean Square Errors for the Seattle data fusion models.

Contribution	HPF	MLT	BT	PCT	IHS
Urban	16.78	44.16	48.93	0.00	49.68
Urban	32.13	67.38	43.26	17.09	22.43
Urban	11.34	50.06	24.08	1.00	9.47
Urban	18.27	63.56	34.92	9.45	18.34
Urban	7.87	49.99	32.86	17.80	13.00
Urban	42.70	51.87	16.90	8.37	10.65
Urban	19.67	37.28	14.38	33.10	11.68
Water	11.60	31.18	18.16	2.45	12.01
Water	6.98	31.71	17.93	1.91	14.01
Water	6.83	31.68	21.25	0.00	14.01
Water	6.38	31.35	20.05	0.58	13.23
Forest	31.27	76.63	61.13	58.21	35.52
Forest	26.52	70.58	52.50	49.67	27.96
Forest	12.57	51.54	20.98	1.41	12.66
Forest	14.67	46.87	35.63	23.72	25.86
Forest	25.98	70.70	52.19	57.23	27.52
Forest	25.83	68.48	49.19	45.84	25.03
Forest	19.92	66.20	47.69	43.93	23.16
Forest	25.38	67.69	53.04	46.54	27.14
Forest	28.24	72.84	55.57	52.48	30.38
SRMSE	20.58	56.93	37.93	24.78	22.30

from the XS data. Four of the models had low SRMSE for the Laguna Beach scene. The HPF model had the lowest error with a 9.85 SRMSE followed by the BT model (12.85), the PCT model (13.21), and the IHS model (15.79). Again for the Seattle scene, the HPF model had the lowest error of 20.58 SRMSE followed by the IHS model (22.3) and the PCT model (24.78). The MLT model consistently had the highest SRMSE for all scenes. For the overall SRMSE performance, the HPF model had the lowest average SRMSE (18.98) followed by the IHS model (19.85).

Landscape contribution to the SRMSE can also be evaluated by analyzing the individual point contribution to the overall SRMSE. With the exception of the MLT model, each model maintains spectral response well for certain landscape features. For the Blacksburg scene, the IHS model has the lowest average SRMSE for urban landscapes and the HPF model has the lowest average for forested landscapes and agricultural plots. The Laguna Beach scene results show the HPF model has the lowest average error for urban, the BT for soil, and the PCT for dark objects such as the fire scars and water, and the IHS for agricultural plots. As noted above, four models had low

Table 14: Summary of Statistical Results by model as compared with each scene’s original XS image

	Correlation			Similar Variance and Means (F-test)			SRMSE
	1	2	3	1	2	3	Error
HPF-Band							
Blacksburg	.73	.72	.81	No	Yes	Yes	26.51
Laguna Beach	.73	.77	.73	No	No	Yes	9.85
Seattle	.70	.70	.69	No	No	Yes	20.85
MLT-Band	1	2	3	1	2	3	Error
Blacksburg	.90	.89	.86	No	No	No	63.79
Laguna Beach	.94	.94	.84	Yes	No	No	33.40
Seattle	.90	.87	.78	No	No	No	56.93
BT-Band	1	2	3	1	2	3	Error
Blacksburg	.84	.88	.86	Yes	Yes	No	51.88
Laguna Beach	.87	.93	.90	No	Yes	Yes	12.85
Seattle	.80	.89	.88	Yes	Yes	No	37.93
PCT-Band	1	2	3	1	2	3	Error
Blacksburg	.89	.93	.75	Yes	Yes	No	35.73
Laguna Beach	.89	.89	.90	Yes	Yes	No	9.85
Seattle	.88	.88	.65	Yes	Yes	No	24.78
IHS-Band	1	2	3	1	2	3	Error
Blacksburg	.80	.87	.85	No	No	Yes	21.46
Laguna Beach	.87	.93	.90	No	No	No	15.79
Seattle	.87	.93	.93	No	Yes	Yes	22.30

SRMSE for the Laguna beach scene showing relatively good performance for the HPF, BT, PCT, and IHS models. For the Seattle scene, the PCT model had the lowest average SRMSE for water and urban landscapes. While the HPF model performed the best for the urban forested landscape. Due to the decrease in brightness values shown in the MLT model, it did not have a low SRMSE for

any of the individual landscapes. Thus, the HPF, IHS, PCT models, and for certain features the BT model, maintain the spectral response of particular landscapes shown by the low SRMSE values.

The statistical measures implemented show certain trends that should be highlighted (Table 14). The IHS and HPF models maintain the best overall correlation between channels with the BT and PCT model showing good correlation between channels. When compared with the original XS data, the MLT shows good correlation with band 1 while the IHS model maintains good correlation among all channels. For overall SRMSE, the HPF model and the IHS model have the lowest overall and per scene SRMSE followed by the PCT model. The BT model did have a low SRMSE for the Laguna Beach scene but this is not reflected in the other two scenes. Statistically, the HPF and IHS models are the best overall data fusion models, followed by the PCT model and the BT model.

Graphical Measures

Figures 29, 30, 31 are feature space plots showing the original XS data alongside the five data fusion models for each scene. Feature space plots showing band 2 on the Y axis and band 3 on the X axis were used to understand the distribution of BV's in feature space.

Figure 29: Feature space plots of band 2 versus band 3 of the Blacksburg data fusion models as compared with the original data.

Figure 30: Feature space plots of band 2 versus band 3 of the Laguna Beach data fusion models as compared with the original data.

Figure 31: Feature space plots of band 2 versus band 3 of the Seattle data fusion models as compared with the original data.

As can be seen by the feature space plots, each of the data fusion models tends to modify the distribution of brightness values. The IHS model for all scenes has similar distribution of pixels as compared with the XS data. Within the distribution though, it tends to eliminate brightness values in a systematic linear fashion. This is possibly a function of the histogram matching of the panchromatic data to the intensity channel. The BT model decreases brightness values, but maintains the general distribution of the XS data for all the scenes. The PCT model has the best relative distribution for the Laguna Beach scene when compared with the XS data, yet also tends to decrease brightness values. The HPF model elongates the distribution for all three scenes and the MLT model decreases brightness values to a very compact distribution.

Figures 32 through 40 show spectral plots of the XS image and the five data fusion models for the three scenes and their dominant landscape features. For urban landscapes on all three scenes the HPF model, with the exception of decreased brightness values, mirrors the XS response. The PCT and IHS model also conserve the urban response quite well. Agricultural landscapes show that the HPF model tends to be similar in the first two channels, but decreases the response of the near infrared channel. The IHS model followed by the PCT model both show similar relative brightness

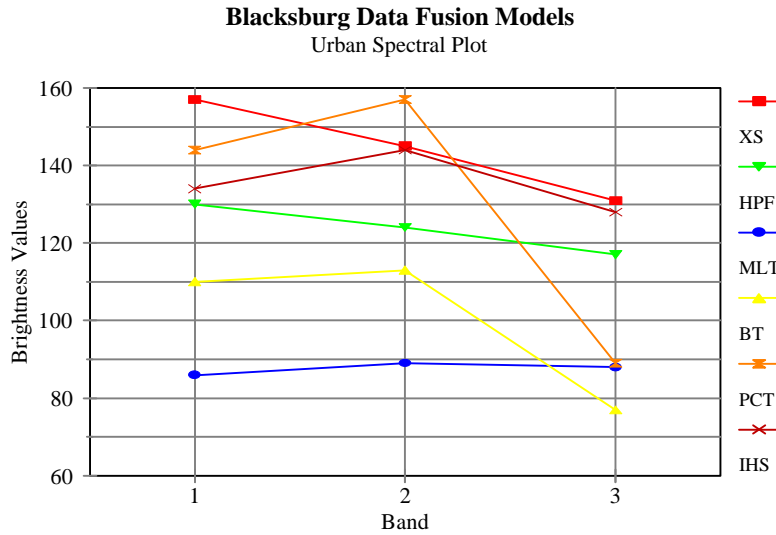


Figure 32: Urban Spectral Plot for Blacksburg data fusion models.

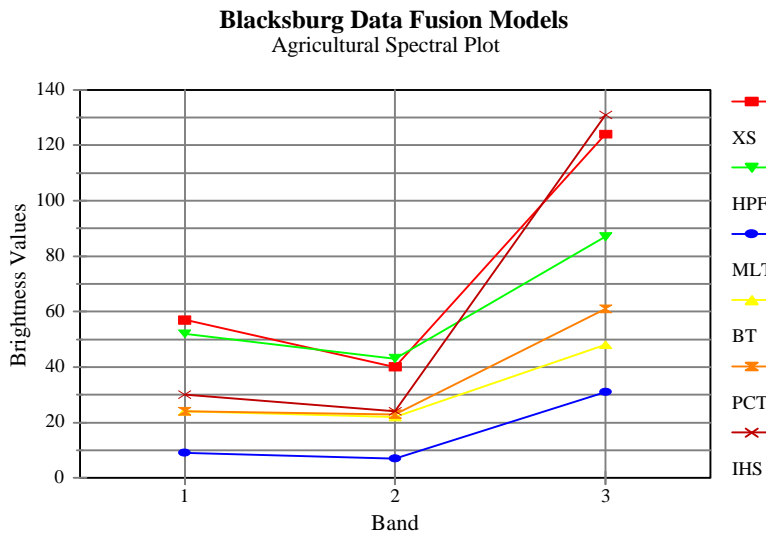


Figure 33: Agricultural Spectral Plot for Blacksburg data fusion models.

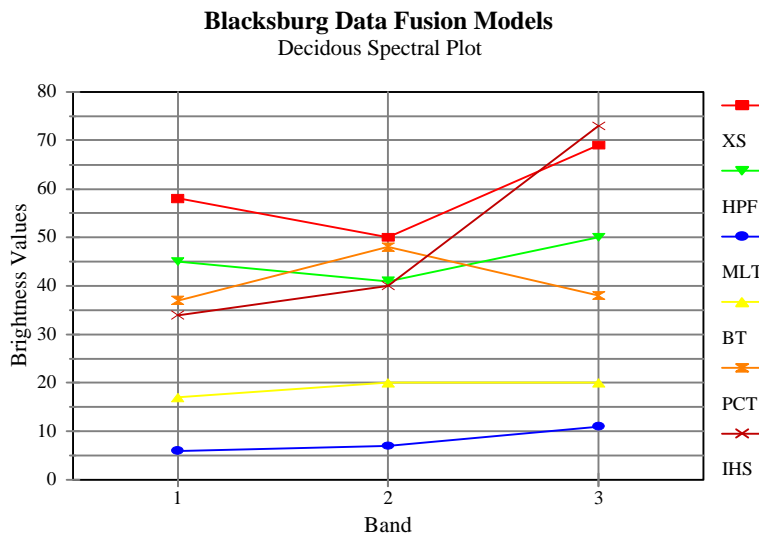


Figure 34: Deciduous forest Spectral Plot for Blacksburg data fusion models.

Laguna Beach Data Fusion Models
Urban Spectral Plot

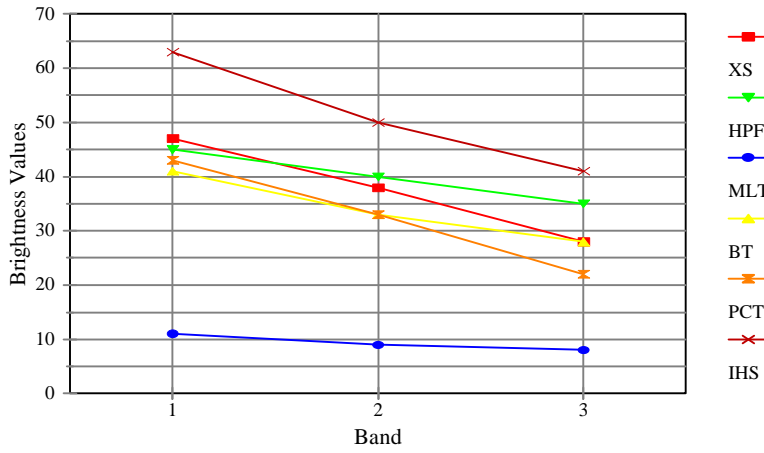


Figure 35: Urban Spectral Plot for Laguna Beach data fusion models.

Laguna Beach Data Fusion Models
Agricultural Spectral Plot

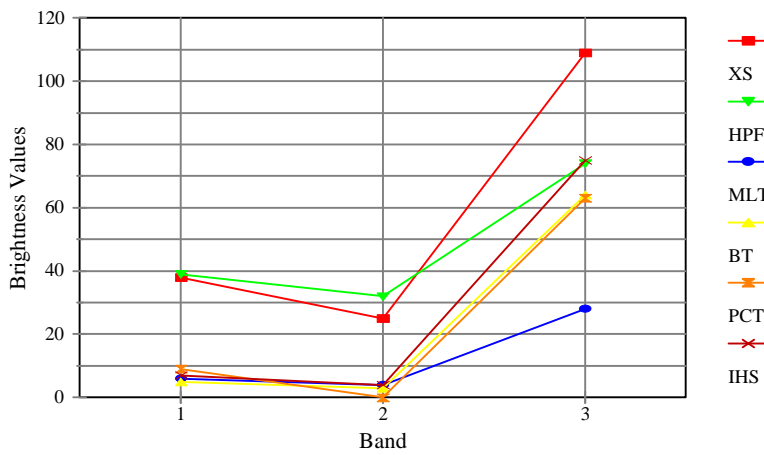


Figure 36: Agricultural Spectral Plot for Laguna Beach data fusion models.

Laguna Beach Data Fusion Models
Water Spectral Plot

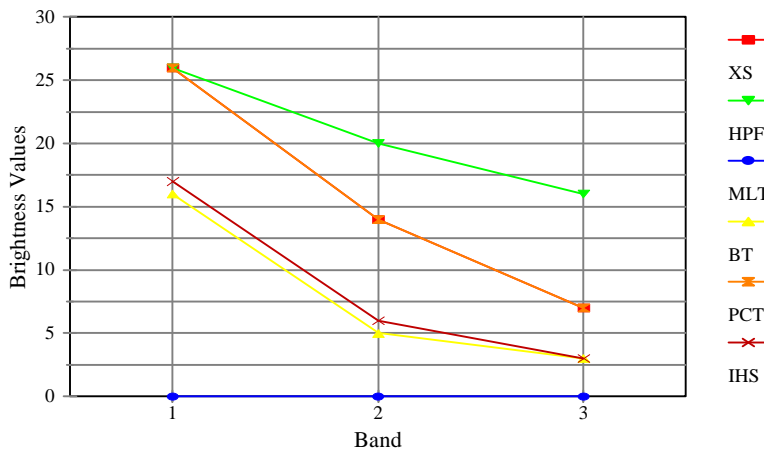


Figure 37: Water Spectral Plot for Laguna Beach data fusion models.

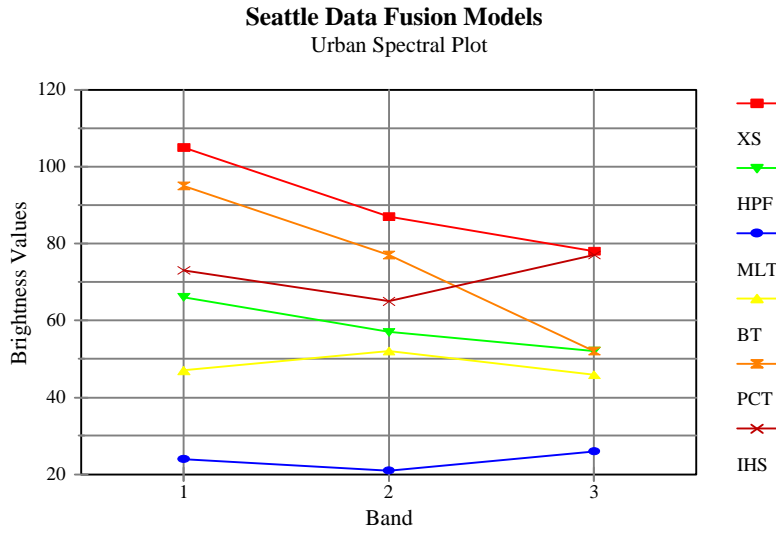


Figure 38: Urban Spectral Plot for Seattle data fusion models.

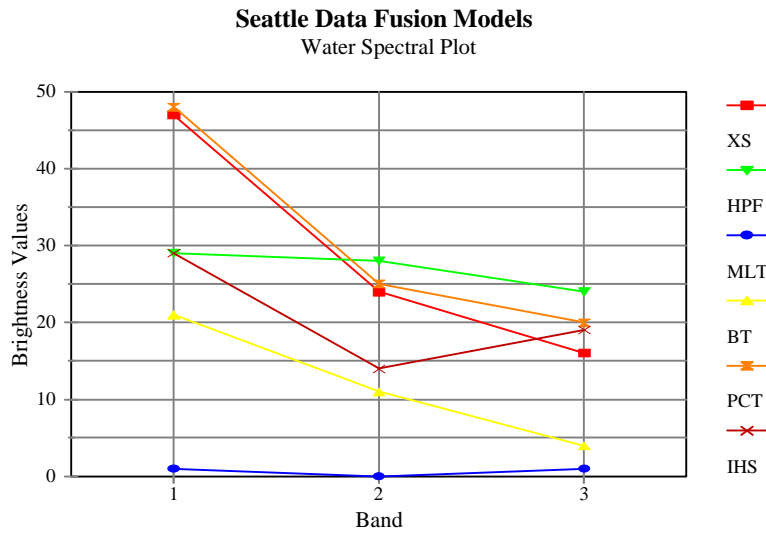


Figure 39: Water Spectral Plot for Seattle data fusion models.

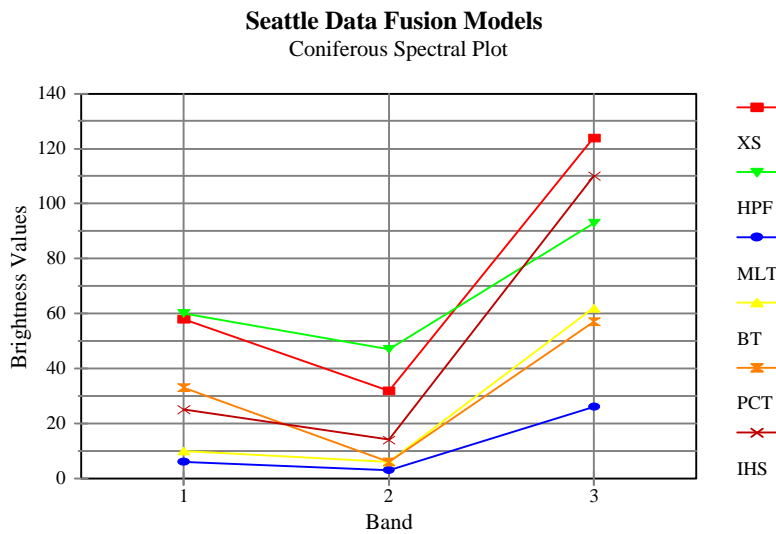


Figure 40: Coniferous Spectral Plot for Seattle data fusion models.

values to the XS data. Forested landscapes show similar responses as to agricultural landscapes with the IHS showing the closest relationship to the XS data. For darker objects such as water as shown in figures 34 and 36, the PCT model is typically exactly the same or very close to the original data. When dark objects are analyzed, the MLT model, with its decreased brightness values, tends to give responses at or near zero. Thus, when analyzed on a point by point spectral response, the IHS, PCT, and HPF models perform the best respectively.

The graphical measures presented techniques to analyze the distribution of brightness values and the spectral response for given landscapes. When analyzed this way the trends seen during the statistical measures are further enhanced. Again the IHS model performs the best followed by the PCT model and the HPF model. For overall spectral integrity these three models maintain the qualities of the original XS data set the best.

Photointerpretive Measures

Up to this point in the analysis all of the analytical techniques have been empirically based. This type of analysis neglects the end means of data fusion techniques, the consumer or user of the final product. Photointerpretive measures provide the scientists from each of the disciplines listed in chapter 3 a chance to evaluate and critique each of the five data fusion models when compared with the original panchromatic and multispectral imagery. Each model was displayed using a linear contrast stretch to remove the effects of the darkening of overall brightness values noted in the preceding statistical and graphical analysis. Table 15 presents the average responses per scene, per model, and overall average and Appendix C presents each of the analyst's responses along with their respective disciplines. It is important to note that although the criterion for each model was not modified for each analyst the differences in perceptual conceptualization did vary with each analyst. This was in part due to the experience each analyst had with analyzing digital data prior to the survey and in part due to the discipline of each of the analyst.

The photointerpretive results presented in Table 15 show that when a linear contrast stretch is applied to each model, the Brovey Transform shows the most overall photointerpretive potential, followed by the High-Pass Filter model and the Intensity-Hue-Saturation model. As can be expected, the HPF model, which highlights the high frequency spatial information of the PN imagery, was consistently rated among the highest for spatial resolution. The BT model corresponded with the original spectral responses of the XS image the best. The IHS model was consistently rated among the top three in all categories by the analysts. The PCT model also was rated high, notably for the Laguna Beach scene, but typically rated below the top three models according to the survey results.

Each of the criterion were then evaluated using an ANOVA, two way without replication, to determine which of the two sources of variation provided the most influence on the analysts responses: variation arising from the different data fusion models (samples) or variation arising from the different scenes (treatments). Tested at the 5 percent level of significance ($\alpha = 0.05$) and an F value of 3.84 for the samples and 4.46 for the treatments for the spatial and spectral criterion the

Table 15: Per scene, per model, and average overall responses for the photointerpretive survey.

Blacksburg					
Mean	HPF	MLT	BT	PCT	IHS
Spatial	94.30	78.60	87.90	68.90	85.30
Spectral	84.30	83.20	93.10	83.80	87.70
Potential	88.50	79.90	88.30	72.00	88.20
Average	89.03	80.57	89.77	74.90	87.07
Laguna Beach					
Mean	HPF	MLT	BT	PCT	IHS
Spatial	89.00	75.50	92.40	89.60	88.30
Spectral	78.60	81.60	91.00	92.30	90.80
Potential	85.50	82.90	87.30	83.40	85.50
Average	84.37	80.00	90.23	88.43	88.20
Seattle					
Mean	HPF	MLT	BT	PCT	IHS
Spatial	91.60	74.20	87.10	79.80	77.00
Spectral	76.00	79.80	90.00	78.70	84.60
Potential	86.60	85.60	91.00	80.50	83.10
Average	84.73	79.87	89.37	79.67	81.57
Overall					
Mean	HPF	MLT	BT	PCT	IHS
Spatial	91.63	76.10	89.13	79.43	83.53
Spectral	79.63	81.53	91.37	84.93	87.70
Potential	86.87	82.80	88.87	78.63	85.60
Average	86.04	80.14	89.79	81.00	85.61

ANOVA proved that the source of variation provided by the models was more prevalent than that provided by the scenes. For the spatial resolution variable, the critical F value for the data fusion models was 3.98 and for the scenes was 1.10. For the spectral quality variable, the F value for the models was 6.44 and for the scenes was 3.78. For the photointerpretive variable, the F value for the models was 3.77 and for the scenes was 0.43 (Appendix D). For the Photointerpretive potential, eventhough the F value for the models was not statistically significant it was still higher than that of the F value for the scenes. This shows that the variance of the responses of each analyst was influenced more by the model analyzed than by which scene the model was being applied to. The third source of variation, the residual or error variance, proved to be the highest in the analysis of the spatial criterion. This can be explained because it was the most quantitative aspect of the test which was by definition qualitative. Thus, the ANOVA allowed the confidence to claim that when analyzed by the consumer, each of the data fusion models provided the major source of variation while differences between scenes was of less concern.

Conclusion

Each analytical technique presented showed that the IHS and HPF models perform the best overall when analyzed for spectral integrity, while the HPF model was the best overall for spatial enhancement. The PCT model also fairs well overall. When the BT model is stretched to take advantage of the entire radiometric display potential, the analysts surveyed found it to be the best method for spectral integrity. The MLT model did not maintain the spectral integrity desired, but did have good correlation with the original XS image and does enhance the spatial quality of the imagery.

CHAPTER FIVE

CONCLUSIONS

Each of the five data fusion models distorted the original spectral signatures to an extent. The severity of each data fusion model's distortion upon the original spectral response can be analyzed using several analytical techniques as seen in Chapter Four. With the exception of the MLT model, each model maintained the spectral integrity of certain landscapes. Yet, the preceding analysis showed that the IHS and HPF models were consistently the best overall method for preservation of spectral integrity. This is not to say that the IHS and HPF models do not have their downfalls, but rather that they minimize the distortion of the original spectral responses when evaluated statistically, graphically, and visually.

When using a data fusion model, the consumer should be able to determine the acceptable level of distortion. Figure 41 presents a simplified data fusion flow chart that provides some basic steps and questions in the decision making process of how to decide on which model is best. The basic question is, "what are the spatial requirements?" Since this study used the SPOT data sets, high spatial resolution is considered to be less than or equal to ten meters and higher than ten meters considered low spatial resolution. Essentially, the flow chart provides the logic to determine whether or not an analyst needs to apply data fusion techniques or use either the XS or PN imagery as stand alone data sets. Within the flow chart are four spectral integrity levels (low, moderate, high, and absolute) which are based upon the analysis within chapter four. As can be seen, the MLT model has low integrity, the BT and PCT models have moderate integrity, and the IHS and HPF models have high integrity. Yet, when absolute spectral integrity is demanded, it is wise to use the XS image alone.

Figure 41: Data Fusion Flow Chart

Table 16 presents the potential use for each data fusion model based on their performance in the preceding analysis. Table 16 is a summary of the results of chapter four and expands upon the integrity levels of the data fusion flow chart. The ratings are based on the spatial and spectral requirements for each application listed in Chapter One within a scale of 0 to 10, with 0 being the least suitable and 10 being highly suitable to an application. Spatial and spectral requirements are weighted equally providing for half of the rating. The spatial rating is based mainly on the photointerpretive results, even though the theoretical ground distance for each pixel is ten meters. The spectral rating is based on the combined results of the analytical techniques presented in Chapter Four. This table provides analysts with a reference for future use of data fusion techniques.

As can be noted, the best models for preservation of spectral response are the IHS and HPF models. The HPF model provides the best spatial enhancement and would be most applicable for

Table 16: Potential application of data fusion techniques.

Model	Environment	*Planning			Forestry	Agriculture	Geology	Cartography
		U	RE	RU				
HPF	8	10	10	10	8	8	10	10
MLT	5	8	8	8	5	5	7	8
BT	7	9	9	9	7	7	8	9
PCT	7	9	9	9	7	7	8	8
IHS	8	9	9	9	8	8	9	9

*Planning subgroups

U-Urban

RE-Regional

RU-Rural

**Ratings

10-High Potential

O-Not advisable

disciplines where spatial enhancement is demanded such as planning, geology, and cartography. For geologic and cartographic applications, all data fusion techniques can be implemented, although some exception might be noted for topographic mapping where vegetation is of concern--then the PCT and BT models should be considered only as alternatives and the MLT technique should not be used. Planning applications for data fusion, particularly for urban and regional planning, are highly focused on infrastructure aspects and thus all techniques can be effectively implemented. The exceptions being rural and to an extent regional planning where as often is the case agriculture and forest lands are of concern and high spectral integrity is needed. For these cases the analyst should consult the environmental section of the table. The applications where spectral integrity is of the most importance, environmental, forestry and agriculture, are highly constrained by which technique can be used. This is due to the need to distinguish between spectral signatures of plant species, delineation of wetlands, and applications of Vegetation Indices (VI). For environmental, forestry and agricultural applications the most practical data fusion techniques are the IHS and HPF models. It is also important for the analyst to realize that none of the data fusion techniques preserve the spectral responses perfectly.

Table 16 reflects only the disciplines discussed in chapter one that may benefit from the use of multispatial imagery and applicable data fusion techniques. Table 16 is meant as a guide and not an authoritative listing, as image processing software and data fusion techniques are created and enhanced, this table can be modified to include improvements in current techniques and the addition of new techniques. Although data fusion is an area of digital remote sensing that has been explored extensively in academia, it, as well as other digital techniques, is constantly being improved and updated. The potential for data fusion is especially applicable considering the advent of the

commercial high spatial resolution satellites scheduled for launch within the next few years. Thus, the need for data fusion techniques to not only provide optimum spatial resolution imagery and maintain spectral integrity of multispectral data is necessary.

Conclusion

While each of the data fusion techniques analyzed here enhanced the spatial resolution of the original XS image, none maintained complete spectral integrity. This is not to say that the application of data fusion to disciplines requiring high spatial integrity cannot benefit from the use of the models, specifically the IHS and the HPF model, it is to say that the analyst should be aware of the benefits as well as the spectral distortion caused by applying the techniques. When spectral integrity cannot be lost then the analyst should regard the gain in spatial resolution provided by data fusion as nil. Although, the spatial enhancements provided with a correlated spectral scene can often be of more benefit than that of a relatively low spatial resolution XS image. Thus, the use of data fusion techniques, when two complementary multispectral scenes are available, should be considered as a potential tool for all analysts.

Appendix A: F Test Results

Blacksburg	Mean	Variance	F test (Variance)	F test (means)	Alpha level	Critical Value
XS1	59.45	94.97			1%	1.7
XS2	47.3	110.11			5%	1.46
XS3	82.14	449.17				
HPF1	50.01	176.64	1.859955776	1.36550308		
HPF2	43.94	180.53	1.639542276	1.286124402		
HPF3	61.36	285.12	1.575371773	1.25518058		
MLT1	7.88	32.05	2.963182527	1.720848057		
MLT2	7.84	32.78	3.359060403	1.823734729		
MLT3	17.07	77.72	5.779336078	2.403628118		
BT1	19.65	92.32	1.028704506	1.013527575		
BT2	20.11	99.91	1.102091883	1.045		
BT3	28.7	127.26	3.529545812	1.879432624		
PCT1	36.34	115.52	1.216384121	1.103696099		
PCT2	43.15	156.38	1.420216147	1.197129187		
PCT3	45.06	82.06	5.473677797	2.33995585		
IHS1	37.55	202.07	2.127724545	1.459958932		
IHS2	39.39	236.77	2.150304241	1.472727273		
IHS3	88.96	434.96	1.032669671	1.016299137		

L a g u n a Beach	Mean	Variance	F test (Variance)	F test (means)	Alpha level	Critical Value
XS1	44.68	113.21			1%	1.7
XS2	39.65	181.83			5%	1.46
XS3	44.86	291.23				
HPF1	46.51	328.73	2.903718753	1.703947368		
HPF2	44	371.44	2.042787219	1.42846553		
HPF3	46.6	388.34	1.33344779	1.154657293		
MLT1	11.93	94.73	1.195080756	1.09352518		
MLT2	11.3	95.73	1.899404575	1.379345603		
MLT3	16.17	127.66	2.281294062	1.510619469		
BT1	33.38	258.15	2.280275594	1.510338346		
BT2	31.41	305.4	1.679590827	1.295774648		
BT3	43.2	341.97	1.174226556	1.083772701		
PCT1	37.01	102.51	1.10438006	1.050345508		
PCT2	30	166.82	1.089977221	1.044117647		
PCT3	32.75	159.3	1.828185813	1.352614897		
IHS1	48.78	383.84	3.390513206	1.841165414		
IHS2	45.09	476.8	2.622229555	1.61897702		
IHS3	59.27	536.9	1.843560073	1.35735208		

Seattle	Mean	Variance	F test (Variance)	F test (means)	Alpha level	Critical Value
XS1	66.57	272.22			1%	1.7
XS2	44.96	299.45			5%	1.46
XS3	59.7	1054.78				
HPF1	57.82	687.27	2.524685916	1.589090909		
HPF2	47.06	703.21	2.348338621	1.532947977		
HPF3	54.45	864.33	1.220344082	1.104761905		
MLT1	9.67	124.74	2.182299182	1.477170994		
MLT2	7.58	92.49	3.237647313	1.798336798		
MLT3	14.78	147.82	7.135570288	2.671052632		
BT1	29.35	319.6	1.1740504	1.083636364		
BT2	25.79	362.74	1.211354149	1.101156069		
BT3	35.41	488.62	2.158691826	1.469683258		
PCT1	60.46	374.96	1.377415326	1.173333333		
PCT2	38.74	413.39	1.380497579	1.175144509		
PCT3	44.11	437	2.413684211	1.554066986		
IHS1	49.88	473.89	1.740834619	1.319393939		
IHS2	35.66	411.48	1.374119219	1.17283237		
IHS3	67.42	1074.19	1.018401942	1.008928571		

Appendix B: Photointerpretive Evaluation

Conditions: Given seven data sets of three scenes, one panchromatic, one multispectral, and five data fusion models for each scene, displayed using Erdas Imagine v. 8.2 software, evaluate each of the five data fusion models for spatial resolution as compared with the original panchromatic image, spectral quality as compared with the original multispectral image, and photointerpretive potential as compared with both the original panchromatic and multispectral imagery.

Evaluation:

1. Compare the spatial resolution of the five data fusion models as compared with the spatial resolution of the original panchromatic image for each scene. This is based on a 100-point scale with 0 being a resolution equivalent to the multispectral image and 100 being a resolution equal to the panchromatic imagery.
2. Compare the spectral quality of the five data fusion models as compared with the original multispectral imagery. This is based on a 100-point scale with 0 being very poor and 100 being equal to the original multispectral imagery.
3. Evaluate the photointerpretive potential of the data fusion models as compared with the original panchromatic and multispectral imagery. This is based on a 100-point scale with 0 being a decrease in photointerpretive potential, 50 being equivalent to the panchromatic and multispectral imagery, and 100 being an increase in photointerpretive potential over the panchromatic and multispectral imagery as stand alone data sets.

*Please list responses in the following table.

Location	Evaluation	Model 1	Model 2	Model 3	Model 4	Model 5
Blacksburg	Spatial Resolution					
	Spectral Quality					
	Photointerpretive Potential					
Laguna Beach	Spatial Resolution					
	Spectral Quality					
	Photointerpretive Potential					
Seattle	Spatial Resolution					
	Spectral Quality					
	Photointerpretive Potential					

Appendix C: Results of Photointerpretive Evaluation

Blacksburg	Evaluation	HPF	MLT	BT	PCT	IHS
	1 Spatial	100	77	100	79	100
*Remote Sensing	Spectral	93	98	95	90	100
	Potential	100	98	100	80	100
	2 Spatial	95	85	90	75	80
GIS	Spectral	80	75	90	80	95
	Potential	95	70	90	40	90
	3 Spatial	100	90	95	80	95
Biology	Spectral	100	95	100	95	100
GIS	Potential	100	93	98	85	98
	4 Spatial	100	90	90	20	85
Forestry	Spectral	85	80	100	65	75
GIS	Potential	100	95	100	70	95
	5 Spatial	100	90	90	60	85
Cartography	Spectral	85	80	100	80	85
Agriculture	Potential	100	95	95	70	85
	6 Spatial	90	80	95	80	85
Remote Sensing	Spectral	80	100	100	100	100
Soils	Potential	85	100	100	100	100
	7 Spatial	85	70	95	80	90
Soils	Spectral	60	70	80	85	90
GIS	Potential	50	50	85	75	90
	8 Spatial	98	94	94	90	88
GIS	Spectral	95	89	96	93	92
	Potential	95	93	90	85	89
	9 Spatial	95	90	80	75	75
Soils	Spectral	95	95	90	90	70
	Potential	90	85	85	75	75
	10 Spatial	80	20	50	50	70
GIS	Spectral	70	50	80	60	70
Cartography	Potential	70	20	40	40	60
Blacksburg	Mean	HPF	MLT	BT	PCT	IHS
	Spatial	94.30	78.60	87.90	68.90	85.30
	Spectral	84.30	83.20	93.10	83.80	87.70
	Potential	88.50	79.90	88.30	72.00	88.20
	Average	89.03	80.57	89.77	74.90	87.07

*Specialties of each scientist surveyed.

Laguna Beach	Evaluation	HPF	MLT	BT	PCT	IHS
	1 Spatial	100	95	100	98	98
Remote Sensing	Spectral	100	97	100	99	100
	Potential	100	98	100	80	100
	2 Spatial	95	75	90	95	90
GIS	Spectral	75	80	85	85	90
	Potential	90	80	85	85	90
	3 Spatial	90	95	100	95	90
Biology	Spectral	90	80	85	85	85
GIS	Potential	90	87	93	90	87
	4 Spatial	70	75	100	100	90
Forestry	Spectral	75	80	100	100	90
GIS	Potential	100	95	100	95	95
	5 Spatial	60	70	100	100	95
Cartography	Spectral	60	80	95	100	100
Agriculture	Potential	90	95	100	95	100
	6 Spatial	100	90	100	100	80
Remote Sensing	Spectral	100	80	100	100	100
Soils	Potential	100	90	100	100	80
	7 Spatial	85	60	95	80	85
Soils	Spectral	60	70	80	80	85
GIS	Potential	40	50	85	75	80
	8 Spatial	95	85	94	93	95
GIS	Spectral	96	94	95	94	93
	Potential	95	94	95	94	93
	9 Spatial	95	90	95	95	100
Soils	Spectral	90	95	90	90	85
	Potential	95	80	75	70	70
	10 Spatial	100	20	50	40	60
GIS	Spectral	40	60	80	90	80
Cartography	Potential	55	60	40	50	60
Laguna Beach	Mean	HPF	MLT	BT	PCT	IHS
	Spatial	89.00	75.50	92.40	89.60	88.30
	Spectral	78.60	81.60	91.00	92.30	90.80
	Potential	85.50	82.90	87.30	83.40	85.50
	Average	84.37	80.00	90.23	88.43	88.20

*Specialties of each scientist surveyed.

Seattle	Evaluation	HPF	MLT	BT	PCT	IHS
	1 Spatial	100	8	100	93	90
Remote Sensing	Spectral	100	95	100	93	93
	Potential	100	90	100	93	90
	2 Spatial	75	85	90	90	85
GIS	Spectral	70	75	80	75	85
	Potential	75	80	95	85	90
	3 Spatial	100	95	95	90	85
Biology	Spectral	90	85	95	90	95
GIS	Potential	95	90	95	90	90
	4 Spatial	80	95	95	75	55
Forestry	Spectral	80	95	95	75	55
GIS	Potential	85	95	100	95	90
	5 Spatial	85	95	95	80	60
Cartography	Spectral	60	80	100	75	95
Agriculture	Potential	85	90	100	95	90
	6 Spatial	100	80	90	100	100
Remote Sensing	Spectral	100	100	100	100	100
Soils	Potential	100	100	100	100	100
	7 Spatial	85	60	90	75	80
Soils	Spectral	60	70	85	70	90
GIS	Potential	50	60	85	60	90
	8 Spatial	96	94	91	85	85
GIS	Spectral	85	88	90	89	93
	Potential	91	91	90	87	91
	9 Spatial	95	90	85	80	80
Soils	Spectral	95	90	85	80	80
	Potential	95	90	85	80	80
	10 Spatial	100	40	40	30	50
GIS	Spectral	20	20	70	40	60
Cartography	Potential	90	70	60	20	20
Seattle	Mean	HPF	MLT	BT	PCT	IHS
	Spatial	91.60	74.20	87.10	79.80	77.00
	Spectral	76.00	79.80	90.00	78.70	84.60
	Potential	86.60	85.60	91.00	80.50	83.10
	Average	84.73	79.87	89.37	79.67	81.57

*Specialties of each scientist surveyed.

Overall	Averages	HPF	MLT	BT	PCT	IHS
	1 Spatial	100.00	60.00	100.00	90.00	96.00
Remote Sensing	Spectral	97.67	96.67	98.33	94.00	97.67
	Potential	100.00	95.33	100.00	84.33	96.67
	2 Spatial	88.33	81.67	90.00	86.67	85.00
GIS	Spectral	75.00	76.67	85.00	80.00	90.00
	Potential	86.67	76.67	90.00	70.00	90.00
	3 Spatial	96.67	93.33	96.67	88.33	90.00
Biology	Spectral	93.33	86.67	93.33	90.00	93.33
GIS	Potential	95.00	90.00	95.33	88.33	91.67
	4 Spatial	83.33	86.67	95.00	65.00	76.67
Forestry	Spectral	80.00	85.00	98.33	80.00	73.33
GIS	Potential	95.00	95.00	100.00	86.67	93.33
	5 Spatial	81.67	85.00	95.00	80.00	80.00
Cartography	Spectral	68.33	80.00	98.33	85.00	93.33
Agriculture	Potential	91.67	93.33	98.33	86.67	91.67
	6 Spatial	96.67	83.33	95.00	93.33	88.33
Remote Sensing	Spectral	93.33	93.33	100.00	100.00	100.00
Soils	Potential	95.00	96.67	100.00	100.00	93.33
	7 Spatial	85.00	63.33	93.33	78.33	85.00
Soils	Spectral	60.00	70.00	81.67	78.33	88.33
GIS	Potential	46.67	53.33	85.00	70.00	86.67
	8 Spatial	96.33	91.00	93.00	89.33	89.33
GIS	Spectral	92.00	90.33	93.67	92.00	92.67
	Potential	93.67	92.67	91.67	88.67	91.00
	9 Spatial	95.00	90.00	86.67	83.33	85.00
Soils	Spectral	93.33	93.33	88.33	86.67	78.33
	Potential	93.33	85.00	81.67	75.00	75.00
	10 Spatial	93.33	26.67	46.67	40.00	60.00
GIS	Spectral	43.33	43.33	76.67	63.33	70.00
Cartography	Potential	71.67	50.00	46.67	36.67	46.67
Overall	Mean	HPF	MLT	BT	PCT	IHS
	Spatial	91.63	76.10	89.13	79.43	83.53
	Spectral	79.63	81.53	91.37	84.93	87.70
	Potential	86.87	82.80	88.87	78.63	85.60
	Average	86.04	80.14	89.79	81.00	85.61

*Specialties of each scientist surveyed.

Appendix D: ANOVA: two way without replication ($\alpha = 0.05$)

Anova: Two Way Without Replication Spatial

<i>Summary</i>	<i>Count</i>	<i>Sum</i>	<i>Average</i>	<i>Variance</i>
HPF	3	274.9	91.63	7.02
MLT	3	228.3	76.1	5.11
BT	3	267.4	89.13	8.16
PCT	3	238.3	79.43	107.22
IHS	3	250.6	83.53	34.26
Blacksburg	5	415	83	93.79
Laguna Beach	5	434.8	86.96	43.463
Seattle	5	409.7	81.94	52.208

Analysis of Variance

<i>Source of Variation</i>	<i>SS</i>	<i>df</i>	<i>MS</i>	<i>F</i>	<i>P-value</i>	<i>F-crit</i>
Rows	504.29	4	126.07	3.98	0.05	3.84
Columns	70.01	2	35.00	1.10	0.38	4.46
Error	253.56	8	31.69			
Total	827.85	14				

Anova: Two Way Without Replication Spectral

<i>Summary</i>	<i>Count</i>	<i>Sum</i>	<i>Average</i>	<i>Variance</i>
HPF	3	238.9	79.63	18.02
MLT	3	244.6	81.53	2.89
BT	3	274.1	91.37	2.50
PCT	3	254.8	84.93	47.20
IHS	3	263.1	87.7	9.61
Blacksburg	5	432.1	86.42	16.997
Laguna Beach	5	434.3	86.86	39.538
Seattle	5	409.1	81.82	30.582

Analysis of Variance

<i>Source of Variation</i>	<i>SS</i>	<i>df</i>	<i>MS</i>	<i>F</i>	<i>P-value</i>	<i>F-crit</i>
Rows	265.93	4	66.48	6.44	0.01	3.84
Columns	77.93	2	38.96	3.78	0.07	4.46
Error	82.54	8	10.32			
Total	426.39	14				

Anova: Two Way
Without Replication PI

<i>Summary</i>	<i>Count</i>	<i>Sum</i>	<i>Average</i>	<i>Variance</i>
HPF	3	260.6	86.87	2.30
MLT	3	248.4	82.8	8.13
BT	3	266.6	88.87	3.66
PCT	3	235.9	78.63	35.10
IHS	3	256.8	85.6	6.51
Blacksburg	5	416.9	83.38	53.82
Laguna Beach	5	424.6	84.92	3.18
Seattle	5	426.8	85.36	15.53

Analysis of Variance

<i>Source of Variation</i>	<i>SS</i>	<i>df</i>	<i>MS</i>	<i>F</i>	<i>P-value</i>	<i>F-crit</i>
Rows	189.52	4	47.38	3.77	0.05	3.84
Columns	10.81	2	5.40	0.43	0.66	4.46
Error	100.61	8	12.58			
Total	300.94	14				

BIBLIOGRAPHY

- Atkinson, P. M. and P. J. Curran, 1997. Choosing an Appropriate Spatial Resolution for Remote Sensing Investigations. *Photogrammetric Engineering and Remote Sensing* 63(12): 1345-1351.
- Campbell, J. B., 1996. *Introduction to Remote Sensing*, 2nd ed. The Guilford Press, 622 p.
- Carper, W. J., T. M. Lillesand, and R. W. Kiefer, 1990. The Use of Intensity-Hue-Saturation Transformations for Merging SPOT Panchromatic and Multispectral Image Data. *Photogrammetric Engineering and Remote Sensing* 56(4): 459-467.
- Chavez, P. S. Jr., 1986. Digital Merging of Landsat TM and Digitized NHAP Data for 1:24,000-Scale Image Mapping. *Photogrammetric Engineering and Remote Sensing* 52(10): 1637-1646.
- Chavez, P. S. Jr., S. C. Sides, and J. A. Anderson, 1991. Comparison of Three Different Methods to Merge Multiresolution and Multispectral Data: Landsat TM and SPOT Panchromatic. *Photogrammetric Engineering and Remote Sensing* 57(3): 295-303.
- Cliche, G. and F. Bonn, 1985. Integration of the SPOT Panchromatic Channel into Its Multispectral Mode for Image Sharpness Enhancement. *Photogrammetric Engineering and Remote Sensing* 51(3): 311-316.
- Colvocoresses, A.P., 1977. Proposed Parameters for an Operational Landsat. *Photogrammetric Engineering and Remote Sensing* 43(9): 1139-1145.
- Conrac Corp., Conrac Division, 1980. *Raster Graphics Handbook*. Covina, CA: Conrac Corp.
- Davis, J.C., 1986. *Statistics and Data Analysis in Geology*, 2nd ed. John Wiley and Sons, Inc., 646 p.
- Daily, M., C. Elachi, T. Farr, W. Stromberg, S. Williams, and G. Schaber, 1978. *Application of Multispectral Radar and Landsat Imagery to Geologic Mapping in Death Valley*, NASA's Jet Propulsion Laboratory Publication 78-19, 47 p.
- Erdas, Inc., 1994. *Erdas Field Guide* 3rd edition. Atlanta, GA: Erdas Inc.
- Ford, S. J. and D. M. Mckeown, Jr., 1992. Information Fusion of Multispectral Imagery for Cartographic Feature Extraction. Invited paper in *Commission VII: Interpretation of Photographic and Remote Sensing Data*. XVII ISPRS Congress.

- Grasso, D. N., 1993. Application of the IHS Color Transformation for 1:24,000-Scale Geologic Mapping: A Low Cost SPOT Alternative. *Photogrammetric Engineering and Remote Sensing* 59(1): 73-80.
- Jensen, J. R., 1996. *Introductory Digital Image Processing: A Remote Sensing Perspective*, 2nd ed. Prentice Hall, 316 p.
- Munichika, C. K., J. S. Warnick, C. Salvaggio, and J. R. Schott, 1993. Resolution Enhancement of Multispectral Image Data to Improve Classification Accuracy. *Photogrammetric Engineering and Remote Sensing* 59(1): 67-72.
- Pellemans, A. H. J. M., R. W. L. Jordans, and R. Allewijn, 1993. Merging Multispectral and Panchromatic SPOT Images with Respect to the Radiometric Properties of the Sensor. *Photogrammetric Engineering and Remote Sensing* 59(1): 81-87.
- Pohl, C. and J. L. van Genderen, 1995. Image Fusion of Microwave and Optical Remote Sensing Data for Topographic Map Updating in the Tropics. *Image and Signal Processing for Remote Sensing II*, 2579: 2-10.
- Robinson, A. H., J. L. Morrison, P. C. Muehrcke, A. J. Kimerling, S. C. Guptill, 1995. *Elements of Cartography*, 6th ed. John Wiley & Sons, INC, 674 p.
- Schott, J.R., 1997. *Remote Sensing: The Image Chain Approach*. Oxford University Press, 394 p.
- Schowengerdt, R. A. 1980. Reconstruction of Multispatial, Multispectral Image Data Using Spatial Frequency Content. *Photogrammetric Engineering and Remote Sensing* 46(10): 1325-1334.
- 1997. *Remote Sensing: Models and Methods for Image Processing*, 2nd ed. Academic Press, 522 p.
- Strahler, A. H., C. E. Woodcock, and J. A. Smith, 1986. On the Nature of Models in Remote Sensing. *Remote Sensing of Environment* 20: 121-139.
- Welch, R. and M. Ehlers, 1987. Merging Multiresolution SPOT HRV and Landsat TM Data. *Photogrammetric Engineering and Remote Sensing* 53(3): 301-303.
- Woodcock, C. E. and A. H. Strahler, 1987. The Factor of Scale in Remote Sensing. *Remote Sensing of Environment* 21: 311-332.
- Wynne, R.H. and D.B. Carter, 1997. Will Remote Sensing Live Up to its Promise for Forest Management? *Journal of Forestry* 95(10): 23-26.

Yesou, H., Y. Besnus, and J. Rolet. Extraction of Spectral Information from Landsat TM Data and Merger with SPOT Panchromatic Imagery--A Contribution to the Study of Geological Structures. *ISPRS Journal of Photogrammetry and Remote Sensing* 48(5): 23-26.

Vita

Duane B. Carter

Duane B. Carter attended Hermiston Senior High School in Hermiston, Oregon, graduating in 1988. He served four years in the United States Army which included a tour of duty in the Republic of Korea and deployment to the Persian Gulf during both Operation Desert Shield and Desert Storm. He received an Associate of Arts from Blue Mountain Community College in June of 1994 and a Bachelor of Science from Portland State University in June of 1996. He is dedicated to the study and teaching of physical geography and geographic technologies toward a better understanding of natural resources.